bioRxiv preprint doi: https://doi.org/10.1101/2020.09.22.308338; this version posted September 22, 2020. The copyright holder for this preprint (which was not certified by peer review) is the author/funder, who has granted bioRxiv a license to display the preprint in perpetuity. It is made available under aCC-BY-NC-ND 4.0 International license.

# NeutrobodyPlex - Nanobodies to monitor a SARS-CoV-2 neutralizing immune response

*Teresa R. Wagner[1,2], Philipp D. Kaiser[2], Marius Gramlich[2], Matthias Becker[2], Bjoern Traenkle[2], Daniel Junker[2], Julia Haering[2], Stefan Nueske[3], Armin Scholz[3], Anne Zeck[2], Katja Schenke-Layland[2,4,6,7], Annika Nelde[8,9],* Monika Strengert[11,12], *Gérard Krause[11,12], Juliane S. Walz[4,8,9,10], Natalia Ruetalo[5], Michael Schindler[5], Nicole Schneiderhan-Marra[2] and Ulrich Rothbauer[1,2#]*

Addresses

[1] Pharmaceutical Biotechnology, Eberhard Karls University Tuebingen, Germany

[2] Natural and Medical Sciences Institute at the University of Tuebingen, Germany

[3] Livestock Center of the Faculty of Veterinary Medicine, Ludwig Maximilians University Munich, Oberschleissheim, Germany

[4] Cluster of Excellence iFIT (EXC2180) “Image-Guided and Functionally Instructed Tumor Therapies”, University of Tuebingen, Tuebingen, Germany

[5] Institute for Medical Virology and Epidemiology of Viral Diseases, University Hospital, Tuebingen, Germany

[6] Department of Women’s Health, Research Institute for Womens’s Health, Eberhard-Karls-University, Tuebingen, Germany

[7] Department of Medicine/Cardiology, Cardiovascular Research Laboratories, David Geffen School of Medicine at UCLA, Los Angeles, CA, USA

[8] Clinical Collaboration Unit Translational Immunology, German Cancer Consortium (DKTK), Department of Internal Medicine, University Hospital Tuebingen, Tuebingen, Germany

[9] Institute for Cell Biology, Department of Immunology, University of Tuebingen, Tuebingen, Germany

[10] Department of Hematology, Oncology, Clinical Immunology and Rheumatology, University Hospital Tuebingen, Tuebingen, Germany

[11] Department of Epidemiology, Helmholtz Centre for Infection Research, Braunschweig, Germany

bioRxiv preprint doi: https://doi.org/10.1101/2020.09.22.308338; this version posted September 22, 2020. The copyright holder for this preprint (which was not certified by peer review) is the author/funder, who has granted bioRxiv a license to display the preprint in perpetuity. It is made available under aCC-BY-NC-ND 4.0 International license.

[12] TWINCORE GmbH, Centre for Experimental and Clinical Infection Research, a joint venture of the Hannover Medical School and the Helmholtz Centre for Infection Research, Hannover, Germany

# corresponding author

Correspondence:
Prof. Dr. Ulrich Rothbauer, Natural and Medical Sciences Institute at the University of Tuebingen
Markwiesenstr. 55, 72770 Reutlingen, Germany.
E-mail: ulrich.rothbauer@uni-tuebingen.de
Phone: +49 7121 51530-415
Fax: +49 7121 51530-816
Ocrid ID: 0000-0001-5923-8986

bioRxiv preprint doi: https://doi.org/10.1101/2020.09.22.308338; this version posted September 22, 2020. The copyright holder for this preprint (which was not certified by peer review) is the author/funder, who has granted bioRxiv a license to display the preprint in perpetuity. It is made available under aCC-BY-NC-ND 4.0 International license.

**Abstract**

Facing the worldwide disease progression of COVID-19 caused by the SARS-CoV-2 virus, the situation is highly critical and there is an unmet need for effective vaccination, reliable diagnosis and therapeutic intervention. Neutralizing binding molecules such as antibodies or derivatives thereof have become important tools for acute treatment of COVID-19. Additionally, such binders provide the unique possibility to monitor the emergence and presence of a neutralizing immune response in infected or vaccinated individuals. Here we describe a set of 11 unique nanobodies (Nbs), originated from an immunized alpaca which bind with high affinities to the glycosylated SARS-CoV-2 Spike receptor domain (RBD). Using a multiplex *in vitro* binding assay we showed that eight of the selected Nbs effectively block the interaction between RBD, S1-domain and homotrimeric Spike protein with the angiotensin converting enzyme 2 (ACE2) as the viral docking site on human cells. According to competitive binding analysis and detailed epitope mapping, we grouped all Nbs blocking the RBD:ACE2 interaction in three distinct Nb-Sets and demonstrated their neutralizing effect with $IC_{50}$ values in the low nanomolar range in a cell-based SARS-CoV-2 neutralization assay. Tested Nb combinations from different sets showed substantially lower $IC_{50}$ values in both functional assays indicating a profound synergistic effect of Nbs simultaneously targeting different epitopes within the RBD. Finally, we applied the most potent Nb combinations in a competitive multiplex binding assay which we termed NeutrobodyPlex and detected a neutralizing immune response in plasma samples of infected individuals. We envisage that our Nbs have a high potential for prophylactic as well as therapeutic options and provide a novel approach to screen for a neutralizing immune response in infected or vaccinated individuals thus helping to monitor the immune status or to guide vaccine design.

bioRxiv preprint doi: https://doi.org/10.1101/2020.09.22.308338; this version posted September 22, 2020. The copyright holder for this preprint (which was not certified by peer review) is the author/funder, who has granted bioRxiv a license to display the preprint in perpetuity. It is made available under aCC-BY-NC-ND 4.0 International license.

## Introduction

The pandemic of Corona Virus Disease 2019 (COVID-19) has been a tremendous wakeup call as we are currently faced with a highly contagious virus that per mid-September 2020 has caused the death of more than 900,000 people world-wide. Facing the current lack of cure or approved vaccine most countries suffer from severe lockdowns and dramatic economic losses. Neutralizing antibodies targeting the causative agent of the disease, the severe acute respiratory syndrome coronavirus 2 (SARS-CoV-2), gain substantial interest for prophylactic and therapeutic options and could help guide vaccine design [1]. These antibodies prevent cellular entry by binding to the docking site of the virus. The SARS-CoV-2 virus binds to the angiotensin converting enzyme II (ACE2) present on human lung epithelium via its receptor binding domain (RBD) located within the homotrimeric transmembrane Spike glycoprotein (Spike) forming a "large-area" interaction site [2]. Since the outbreak of the COVID-19 pandemic, a constantly growing number of neutralizing antibodies targeting the RBD of SARS-CoV-2 has been identified from COVID-19 patients [1, 3] underlining the importance of RBD-specific antibodies blocking the RBD:ACE2 interaction site for the development of a protective immune response [4]. A promising alternative to conventional antibodies (IgGs) are single-domain antibodies (nanobodies, Nbs) derived from the heavy-chain antibodies of camelids (**Figure 1**). Due to their small size and compact folding Nbs show a high chemical stability, solubility and fast tissue penetration. Employing a targeted screening approach Nbs can be selected against different epitopes on the same antigen and easily converted into multivalent formats [5]. In comparison to antibodies Nbs have similar specificities and affinities and, due to their high homology with human antibody (VH) fragments they show only very low immunogenicity. With VHH-72 the first cross-reactive Nb which binds the RBD of SARS-CoV-1 as well as of SARS-CoV-2 was recently reported [6]. Since this first publication, several SARS-CoV-2 RBD specific Nbs were identified from naïve/ synthetic libraries [7-9] or immunized animals [10-14]. However, to date only very few Nbs were identified displaying high affinities in the monovalent format [8, 10]. Most of them have to be converted into multivalent formats or applied as Fc fusion to efficiently block virus entry [6, 7]. This limits the developability

bioRxiv preprint doi: https://doi.org/10.1101/2020.09.22.308338; this version posted September 22, 2020. The copyright holder for this preprint (which was not certified by peer review) is the author/funder, who has granted bioRxiv a license to display the preprint in perpetuity. It is made available under aCC-BY-NC-ND 4.0 International license.

and applicability of those binders since protein size is distinctly increased and furthermore Fc fusions bear the risk of unwanted antibody-dependent enhancement (ADE) in patients. Additionally, the observed high mutation rate of SARS-CoV-2 [15, 16] further stresses the need of selecting high affinity Nbs addressing multiple epitopes within the RBD to ensure sufficient neutralization potency of virus harboring sequential and/ or structural changes in their docking site.

Here we describe the selection of 11 unique Nbs, from a Nb gene library derived from an alpaca immunized with glycosylated SARS-CoV-2 RBD. All Nbs can be readily produced in bacteria at high yields and bind their target structure with strong affinities in their monovalent format. Eight of the selected Nbs effectively block the interaction between RBD, S1-domain and the homotrimeric Spike protein with ACE2 as the viral docking site in a multiplex *in vitro* binding assay. Based on competitive binding analysis and detailed epitope mapping using Hydrogen Deuterium Exchange mass spectrometry (HDX-MS) we clustered all ACE2 blocking Nbs in three distinct Nb-Sets and demonstrated their potential to neutralize SARS-CoV-2 infection in a human cell model. By testing combinations from different Nb-Sets in both functional assays, we achieved substantially improved $IC_{50}$ values indicating a highly synergistic effect of Nbs targeting simultaneously different epitopes within the RBD. Finally, we performed a competitive binding assay, which we termed NeutrobodyPlex, using serum samples from infected individuals and the most potent inhibitory Nb combinations. With this approach we demonstrated the presence of antibodies in patient samples addressing the RBD:ACE2 interface which are in accordance to previous findings designed as being neutralizing antibodies. Based on the data presented here, we propose, that our Nbs have a high potential for prophylactic and therapeutic options and provide a novel high-throughput approach to screen for a neutralizing immune response in infected or vaccinated individuals thus helping to monitor the immune status or to guide vaccine design.

bioRxiv preprint doi: https://doi.org/10.1101/2020.09.22.308338; this version posted September 22, 2020. The copyright holder for this preprint (which was not certified by peer review) is the author/funder, who has granted bioRxiv a license to display the preprint in perpetuity. It is made available under aCC-BY-NC-ND 4.0 International license.

## Results

*Selection of Nbs binding to the RBD of SARS-CoV-2*

To generate Nbs directed against the RBD of SARS-CoV-2 we expressed and purified RBD in mammalian (Expi293) cells [17] and immunized an alpaca (*Vicugna pacos*) following a 64-day immunization protocol. Subsequently, we generated a Nb phagemid library comprising ~ 4 x $10^7$ clones representing the full repertoire of the variable heavy chains of heavy-chain antibodies ($V_H$Hs or Nbs) derived from the animal. The library was subjected to phage display and biopanning was performed using either passively adsorbed or biotinylated RBD immobilized on streptavidin plates. After two phage display cycles we analyzed 492 individual clones in a solid-phase phage ELISA and identified 325 positive binders. Sequence analysis of 72 clones revealed 11 unique Nbs which cluster in eight families with highly diverse complementarity determining regions (CDR) 3 (**Figure 2 A**). Individual Nbs were cloned with a C-terminal $His_6$-tag, expressed in *Eschericha coli (E.coli)* and purified using immobilized metal ion affinity chromatography (IMAC) followed by size exclusion chromatography (SEC) (**Figure 2 B**). For affinity measurements, we used biolayer interferometry (BLI) and immobilized biotinylated RBD on the sensor tip. Incubation with serial dilutions of the Nbs revealed $K_D$ values ranging from ~1.3 nM to ~53 nM indicating a strong binding of the Nbs in their monovalent format. NM1225 revealed a binding affinity in the micromolar range and was therefore not considered for further analysis. (**Figure 2 C, Supplementary Figure 1**).

*Nbs compete with ACE2 for binding to RBD, S1 or homotrimeric Spike*

Next we analyzed the potential of the Nbs to block the interaction between homotrimeric Spike, S1 domain or the RBD to ACE2. We utilized an in-house developed multiplex binding assay for which we first covalently coupled the respective SARS-CoV-2 derived proteins on spectrally distinct populations of paramagnetic beads (MagPlex Microspheres) [18]. For parallelized analysis these beads were pooled and simultaneously incubated with biotinylated ACE2 and dilutions of purified Nbs ranging from 2 µM to 12.3 pM. To screen for inhibitory Nbs, residual binding of ACE2 to distinct viral antigens was detected on a Luminex instrument using R-

bioRxiv preprint doi: https://doi.org/10.1101/2020.09.22.308338; this version posted September 22, 2020. The copyright holder for this preprint (which was not certified by peer review) is the author/funder, who has granted bioRxiv a license to display the preprint in perpetuity. It is made available under aCC-BY-NC-ND 4.0 International license.

phycoerythrin (PE)-labeled streptavidin after stringent washing. Additionally, as negative control a non-specific Nb (GFP-Nb) and as positive control two inhibiting mouse antibodies were analyzed [19]. Data obtained by this multiplex binding assay showed that eight of the 10 analyzed Nbs inhibit ACE2 binding to isolated RBD, S1 domain and homotrimeric Spike. $IC_{50}$ values calculated for inhibition of ACE2:RBD interaction ranges between 0.5 nM for NM1228 and 38 nM for NM1229 (**Figure 3**). Notably, $IC_{50}$ values obtained for the most potent inhibitory Nbs NM1228 (0.5 nM), NM1226 (0.85 nM) and NM1230 (2.12 nM) are highly comparable to $IC_{50}$ values measured for the mouse IgGs (40591-MM43: 0.38 nM; 40592-MM57: 3.22 nM). Additionally, the assay revealed that all Nbs except NM1224, show a similarly strong inhibitory effect of ACE2 binding to all tested antigens. NM1224 seems to exclusively inhibit RBD:ACE2 interaction and does not prevent binding of ACE2 to neither homotrimeric Spike nor S1 domain.

*Epitope binning*

After identifying RBD-specific Nbs with inhibitory effect on ACE2 binding, we investigated the relative location of their epitopes within the RBD. Thus, we first performed epitope binning experiments of Nb combinations using BLI. After coating sensors with biotinylated RBD, a first Nb was loaded until binding saturation was reached, followed by a short dissociation step to remove excess Nb. A second Nb from a different family was then exposed to the RBD-Nb-complex. Using this approach, we identified Nbs which recognize overlapping and non-overlapping epitopes on RBD (**Figure 4**, **Supplementary Figure 2**). As expected Nbs with only minor differences in their CDR3 (NM1221, NM1222 and NM1230, Nb-Set 2) were suggested to recognize an identical or highly similar epitope as they cannot bind simultaneously to RBD. Interestingly, our analysis revealed that Nbs with highly diverse CDR3s such as NM1228, NM1226, NM1227 and NM1229 also could not bind simultaneously, suggesting that these Nbs recognize similar or at least overlapping epitopes. Accordingly, we clustered these diverse Nbs in Nb-Set 1. In total, based on epitope binning, we identified five distinct Nbs-Sets, comprising at least one candidate targeting a different epitope within the RBD compared to any member of a different Nb-Set (**Figure 4**).

bioRxiv preprint doi: https://doi.org/10.1101/2020.09.22.308338; this version posted September 22, 2020. The copyright holder for this preprint (which was not certified by peer review) is the author/funder, who has granted bioRxiv a license to display the preprint in perpetuity. It is made available under aCC-BY-NC-ND 4.0 International license.

*Epitope mapping of RBD binding Nbs*

We next performed Hydrogen-Deuterium Exchange Mass Spectrometry (HDX-MS) with the most potent inhibitory Nbs selected from the different Nb-Sets to more precisely locate their binding sites at the surface of RBD, and allowing comparison with the RBD:ACE2 interface. Both members of Nb-Set1, NM1226 and NM1228, interacted with the RBD at the back/ lower right site (Back View, **Figure 5**). Notably, the binding site of NM1226 does not encompass amino acid residues involved in the RBD:ACE2 interface. In contrast, NM1228 (Nb-Set1) as well as NM1230 (Nb-Set2) contacted RBD at amino acid residues overlapping with the RBD:ACE2 binding interface, whereas NM1230 additionally covers parts of the spike-like loop region on one edge of the ACE2 interface at the top front/ lower left side (Front View, **Figure 5**). In accordance to our binning studies, Nbs from both Sets do not share overlapping epitopes. As expected, NM1221 and NM1222 (both Nb-Set2) addressed similar RBD regions compared to NM1230 (**Supplementary Figure 3**). NM1224 (Nb-Set4) showed an interaction distinct from all other Nbs covering besides its main binding region located at the lower right side (Front View, **Figure 5**) also residues in the ACE2:RBD interface (upper left corner, Front View, **Figure 5**). As negative control, we analyzed the non-inhibitory NM1223 (Nb-Set3) (**Figure 5**) which did not contact any amino acid residues involved in the RBD:ACE2 interface but rather binds to the opposite site (Front View, **Figure 5**). Comparing the data from epitope binning with the HDX-MS results provides structural insights into the mechanism by which non-competing pairs of Nbs can simultaneously bind the RBD. Interestingly, the combination of NM1228 (Nb-Set1) with NM1230 (Nb-Set2) shows a nearly complete coverage of the ACE2 interface (**Figure 5**) whereas the observed inhibitory effect of NM1226 might be due to steric hindrance. In conclusion, we suppose that the combination of Nb-Set1 with Nb-Set2 acts synergistically on the inhibition of the interaction between RBD and ACE2.

*RBD Nbs can potently neutralize the SARS-CoV-2 virus*

bioRxiv preprint doi: https://doi.org/10.1101/2020.09.22.308338; this version posted September 22, 2020. The copyright holder for this preprint (which was not certified by peer review) is the author/funder, who has granted bioRxiv a license to display the preprint in perpetuity. It is made available under aCC-BY-NC-ND 4.0 International license.

After identification of Nbs which inhibit the RBD:ACE2 interaction biochemically, we employed a cell-based viral infection assay to test for their neutralization potency. Thus, human Caco-2 cells were co-incubated with the icSARS-CoV-2-mNG strain and serial dilutions of the inhibitory Nbs NM1224, NM1226, NM1228 and NM1230. 48 h post-infection neutralization potency was determined via automated fluorescence-microscopy of fixed and nuclear-stained cells. As read-out cell count and infection rate were analyzed from cell images. (**Supplementary Figure 4**). Percentage of infected cells following Nb treatment normalized to a non-treated control was plotted and $IC_{50}$ values were determined via sigmoidal inhibition curve fits as the half-maximal infection. Overall, data obtained from the multiplex binding assay and the viral infection assay revealed a broad consistency. Representatives of Nb-Set1, NM1226 and NM1228, showed the highest neutralization potency with $IC_{50}$ values of ~15 nM and ~7 nM followed by NM1230 (~37 nM) and NM1224 (~256 nM). As expected, NM1223 (Nb-Set3) was not found to reduce viral infectivity.

Considering that Nbs targeting diverse epitopes within the RBD:ACE2 interface are beneficial to pronouncedly reduce viral infectivity and prevent mutational escape, we next combined the most potent inhibitory and neutralizing candidates derived from Nb-Set1 (NM1226, NM1228) and Nb-Set2 (NM1230) and tested them in the multiplex binding assay and for viral neutralization. In the multiplex binding assay the combination of NM1226 and NM1230 showed an increased effect in competing with ACE2 binding to RBD illustrated by a $IC_{50}$ of 0.42 nM which is 2- or 5-fold lower compared to treatment with individual NM1226 or NM1230, respectively (**Figure 7 A**). Notably, the $IC_{50}$ measured for the combination of NM1228 and NM1230 did not exceed the $IC_{50}$ identified for NM1228 alone indicating that NM1228 by its own has a very high inhibiting effect (**Figure 7 A**). When we tested both combinations in the viral infection assay, we observed significantly improved effects for both of them illustrated by an $IC_{50}$ of ~4 nM for the combination NM1226 and NM1230 and ~3.5 nM for NM1228 and NM1230 (**Figure 7 B, Supplementary Figure 5**). From these findings we conclude, that a combinatorial treatment with two Nbs targeting different epitopes within the RBD:ACE2 interaction site is highly beneficial for viral neutralization.

bioRxiv preprint doi: https://doi.org/10.1101/2020.09.22.308338; this version posted September 22, 2020. The copyright holder for this preprint (which was not certified by peer review) is the author/funder, who has granted bioRxiv a license to display the preprint in perpetuity. It is made available under aCC-BY-NC-ND 4.0 International license.

*The NeutrobodyPlex - High-throughput detection of neutralizing antibodies in serum samples of patients after SARS-CoV-2 infection*

Recently, several serological assays analyzing the immune response in infected and recovered SARS-CoV-2 patients have been published [17, 18, 20-22]. These assays provide data on the presence and distribution of antibody subtypes against the SARS-CoV-2 within serum samples. However, while those testing systems detect the overall antibody response against distinct antigens of SARS-CoV-2, they do not provide the answer to the most relevant question whether the tested individuals carry neutralizing antibodies which prevent reinfection. In this context, multiple studies have convincingly shown that neutralizing antibodies preferable bind to the RBD domain and sterically inhibit viral entry via ACE2 [1, 3]. This let us assume that our RBD Nbs covering large parts of the RBD:ACE2 interface might be suitable to monitor the emergence and presence of neutralizing antibodies in patients. To test this hypothesis, we set up a high-throughput competitive binding assay, termed NeutrobodyPlex, by combining our most potent neutralizing Nb combinations with a recently developed, automatable multiplex immunoassay (**Figure 8 A**) [18]. We incubated our previously generated color-coded beads comprising RBD, S1 domain or homotrimeric Spike with serum samples from patients or non-infected individuals in addition to dilution series of the combinations NM1226/ NM1230 or NM1228/ NM1230 followed by the detection of patient-derived IgGs bound to the respective antigens. Depending on the Nb concentration, neutralizing antibodies targeting the RBD:ACE2 interaction site within the serum samples are displaced resulting in a reduction of the detectable signal (**Figure 8 A**).

By analyzing RBD specific IgGs from serum samples, we detected a distinct signal reduction in the presence of increasing Nb concentrations for all tested samples (**Figure 8 B, Supplementary Figure 6 A**) indicating that all patients comprise a substantial fraction of RBD-reactive IgGs targeting the RBD:ACE2 interface. Notably, we observed no changes when analyzing competitive binding for IgGs addressing the homotrimeric Spike protein, which

bioRxiv preprint doi: https://doi.org/10.1101/2020.09.22.308338; this version posted September 22, 2020. The copyright holder for this preprint (which was not certified by peer review) is the author/funder, who has granted bioRxiv a license to display the preprint in perpetuity. It is made available under aCC-BY-NC-ND 4.0 International license.

suggests the presence of multiple IgGs targeting epitopes beyond the RBD:ACE2 interaction site (**Figure 8 B, Supplementary Figure 6 A**).

To further demonstrate that our approach is able to determine the presence of IgGs targeting the RBD:ACE2 interaction site in detailed resolution, we highlighted the effect of competing Nbs on two selected serum samples. For sample #289 we observed a clear displacement of IgGs when we measured antibody binding to RBD and S1 domain upon addition of competing Nbs, while for sample #265 only a slight reduction of the IgG signal on S1 domain was detectable (**Figure 8 C, Supplementary Figure 6 B**). Additionally, we compared our NeutrobodyPlex approach using RBD-specific Nbs with conventional antibodies by applying the neutralizing mouse antibody MM43 [19] in a similar setting. Here we detected substantial cross-reactive signals from the labeled anti-human-IgG in all five serum samples (**Supplementary Figure 6 C**). From those findings we conclude, that mouse antibodies are not suitable, as they bear the risk to be falsely detected. In summary, our data revealed that the NeutrobodyPlex provides a suitable screening system to monitor the presence of RBD-targeting antibodies in patient samples which can be reliably considered to mediate a neutralizing and protective immune response.

Finally, we validated our NeutrobodyPlex by analyzing a cohort of 18 serum samples of convalescent SARS-CoV-2 patients and four control samples from healthy donors using one consistent Nb concentration (1.26 µM). Within the tested serum cohort all donors infected with SARS-CoV-2 showed the presence of neutralizing antibodies, most clearly visible when using RBD as antigen (**Figure 9 A, Supplementary Figure 7**). For direct comparison with the a cell-based viral infection assay as the gold standard for detecting neutralizing serum antibodies [23], we tested the same sample cohort in dilution series using the previously described icSARS-CoV-2-mNG strain in Caco-2 cells (**Figure 9 B**). The viral infection assay revealed the presence of neutralizing antibodies in the same sample set derived from convalescent SARS-CoV-2 patients, whereas none of the samples from healthy donors showed any effect. Observable differences between the patient samples can be explained by different antibody

bioRxiv preprint doi: https://doi.org/10.1101/2020.09.22.308338; this version posted September 22, 2020. The copyright holder for this preprint (which was not certified by peer review) is the author/funder, who has granted bioRxiv a license to display the preprint in perpetuity. It is made available under aCC-BY-NC-ND 4.0 International license.

titers, which were not investigated further. In summary, our findings showed that both screening assays provide consistent information and demonstrate the suitability of our NeutrobodyPlex using RBD as the most relevant antigen to reliably monitor the presence of neutralizing antibodies in patients.

bioRxiv preprint doi: https://doi.org/10.1101/2020.09.22.308338; this version posted September 22, 2020. The copyright holder for this preprint (which was not certified by peer review) is the author/funder, who has granted bioRxiv a license to display the preprint in perpetuity. It is made available under aCC-BY-NC-ND 4.0 International license.

## Discussion

Indisputably, there is a strong need for diagnostic tools and therapeutics against SARS-CoV-2 infection. As demonstrated for neutralizing antibodies selected from convalescent COVID-19 patients, biologically-derived binding molecules can effectively address the large interaction site of the RBD domain of SARS-CoV-2 and the ACE2 receptor exposed on human lung epithelium [3, 24, 25]. A promising alternative to conventional antibodies are Nbs derived either from naïve/ synthetic libraries or immunized camelids [26]. By employing suitable screening strategies, Nbs addressing predefined domains within larger antigens can be selected. Since the description of the first Nb shown to bind the RBD of homotrimeric Spike protein of SARS-CoV-2 [6], multiple well working Nbs targeting this particular viral domain have been identified [7, 8, 10, 11]. In this study we identified 11 novel RBD-specific Nbs derived from an immunized animal (*Vicugna pacos*). According to their sequences these Nbs can be clustered in 8 unique families representing different germ lines which indicates a prominent immune response towards the fully glycosylated antigen. All identified monovalent Nbs except NM1225 showed affinities in the low nanomolar range. Thus, these Nbs do not require reformatting into bivalent formats e.g. by fusing to a Fc domain or by combining multiple binding sites as previously shown for other RBD targeting Nbs [6, 9, 10, 12-14].

For functional analysis we employed a recently developed *in vitro* multiplex binding assay [18] to monitor the replacement of ACE2 as the natural ligand from binding to RBD, S1 domain or homotrimeric Spike upon addition of RBD-specific Nbs. With this assay we were able to identify eight inhibiting Nbs targeting those Spike-derived antigens. Interestingly, $IC_{50}$ values obtained for inhibitory Nbs on RBD and homotrimeric Spike show a higher correlation compared to $IC_{50}$ values obtained for the S1 domain. Based on a detailed epitope mapping, we grouped our Nbs in five different Nb-Sets. Three of those Nb-Sets are comprising inhibitory Nbs, which were shown to target different epitopes within the RBD:ACE2 interaction site. We confirmed the neutralizing potency of those Nbs in a cell-based viral infection assay using fully intact SARS-CoV-2. By this we noted that the measurable viral neutralization effect of the individual Nbs strongly correlates to the data obtained from the biochemical screen, which demonstrates that

bioRxiv preprint doi: https://doi.org/10.1101/2020.09.22.308338; this version posted September 22, 2020. The copyright holder for this preprint (which was not certified by peer review) is the author/funder, who has granted bioRxiv a license to display the preprint in perpetuity. It is made available under aCC-BY-NC-ND 4.0 International license.

the multiplex binding assay as presented is highly relevant and suitable to identify virus neutralizing binders. Based on these findings we modified our previously described multiplex immunoassay (MULTICOV-AB, [18]) and developed a novel diagnostic test called NeutrobodyPlex to monitor the presence and the emergence of neutralizing antibodies in serum samples of SARS-CoV-2 infected individuals. Using combinations of high affinity Nbs covering the RBD:ACE2 interface we were able to directly and specifically displace IgGs present in serum samples from these particular RBD epitopes. According to previous studies human IgGs addressing those epitopes were classified as neutralizing antibodies [1, 24, 25]. In our NeutrobodyPlex we further demonstrated that such neutralizing antibodies can be detected best using the RBD. Larger Spike-derived antigens especially the full length homotrimeric Spike, which is bound by a multitude of different IgGs, could be useful to determine the fraction of neutralizing antibodies in a patient sample. Finally, we validated the suitability of our approach by testing serum samples from 18 patients and four healthy donors in comparison to the classical cell-based viral infection assay. The observed strong accordance between both assays confirmed the ability of the NeutrobodyPlex to precisely monitor the presence of neutralizing antibodies within patient samples.

To our knowledge, the NeutrobodyPlex employing Nbs blocking the RBD:ACE2 interaction site shows for the first time an antigen-resolved analysis of the presence of human IgGs in convalescent individuals suffering from SARS-CoV-2 infection. Compared to other neutralizing serum antibody detection tests, this assay enables the analysis on an automatable high-throughput basis and is performed with non-living and non-infectious viral material thus reducing costs and safety conditions [23, 27]. Furthermore, the NeutrobodyPlex is highly sensitive as low serum dilutions (tested dilution: 1:400) are sufficient for analysis which significantly reduces patient material compared to standard assays. Considering our findings, it is highly conceivable that the NeutrobodyPlex will open unique possibilities for a detailed classification of the individual immune status with regard to the development of protective antibodies and to monitor the efficiency of strongly needed vaccination campaigns.

bioRxiv preprint doi: https://doi.org/10.1101/2020.09.22.308338; this version posted September 22, 2020. The copyright holder for this preprint (which was not certified by peer review) is the author/funder, who has granted bioRxiv a license to display the preprint in perpetuity. It is made available under aCC-BY-NC-ND 4.0 International license.

## Materials and Methods

**Expression constructs** For bacterial expression of Nbs, sequences were cloned into the pHEN6 vector [28], thereby adding a C-terminal 6xHis-tag for IMAC purification as described previously [29, 30]. The pCAGGS plasmids encoding the stabilized homotrimeric Spike protein and the receptor binding domain (RBD) of SARS-CoV-2 were kindly provided by F. Krammer [17]. The cDNA encoding the S1 domain (aa 1 - 681) of the SARS-CoV-2 Spike protein was obtained by PCR amplification using the forward primer S1_CoV2-for 5´- CTT CTG GCG TGT GAC CGG - 3´ and reverse primer S1_CoV2-rev 5´ - GTT GCG GCC GCT TAG TGG TGG TGG TGG TGG TGG GGG CTG TTT GTC TGT GTC TG - 3´ and the full length SARS-CoV-2 Spike cDNA as template and cloned into the XbaI/ NotI-digested backbone of the pCAGGS vector, thereby adding a C-terminal $His_6$-Tag. All expression constructs were verified by sequence analysis.

**$V_HH$ libraries** Alpaca immunizations with purified RBD and $V_HH$-library construction were carried out as described previously [31]. Animal immunization has been approved by the government of Upper Bavaria (Permit number: 55.2-1-54-2532.0-80-14). In brief, nine weeks after immunization of an animal (*Vicugna pacos*) with either C-terminal histidine-tagged RBD (RBD-$His_6$), ~100 ml blood were collected and lymphocytes were isolated by Ficoll gradient centrifugation using the Lymphocyte Separation Medium (PAA Laboratories GmbH). Total RNA was extracted using TRIzol (Life Technologies) and mRNA was reverse transcribed to cDNA using a First-Strand cDNA Synthesis Kit (GE Healthcare). The $V_HH$ repertoire was isolated in 3 subsequent PCR reactions using following primer combinations (1) CALL001 (5´-GTC CTG GCT GCT CTT CTA CA A GG-3´) and CALL002 (5´-GGT ACG TGC TGT TGA ACT GTT CC-3´) (2) forward primer set FR1-1, FR1-2, FR1-3, FR1-4 (5´-CAT GGC NSA NGT GCA GCT GGT GGA NTC NGG NGG-3´, 5´-CAT GGC NSA NGT GCA GCT GCA GGA NTC NGG NGG-3´, 5´-CAT GGC NSA NGT GCA GCT GGT GGA NAG YGG NGG-3´, 5´-CAT GGC NSA NGT GCA GCT GCA GGA NAG YGG NGG-3´) and reverse primer CALL002 and (3) forward primer FR1-ext1 and FR1-ext2 (5´-GTA GGC CCA GCC GGC CAT GGC NSA NGT GCA GCT

bioRxiv preprint doi: https://doi.org/10.1101/2020.09.22.308338; this version posted September 22, 2020. The copyright holder for this preprint (which was not certified by peer review) is the author/funder, who has granted bioRxiv a license to display the preprint in perpetuity. It is made available under aCC-BY-NC-ND 4.0 International license.

GGT GG-3`, 5`-GTA GGC CCA GCC GGC CAT GGC NSA NGT GCA GCT GCA GGA-3´ A-) and reverse primer set FR4-1, FR4-2, FR4-3, FR4-4, FR4-5 and FR4-6 (5`-GAT GCG GCC GCN GAN GAN ACG GTG ACC NGN RYN CC-3´. 5`-GAT GCG GCC GCN GAN GAN ACG GTG ACC NGN GAN CC-3´. 5`-GAT GCG GCC GCN GAN GAN ACG GTG ACC NGR CTN CC-3´. 5`-GAT GCG GCC GCR CTN GAN ACG GTG ACC NGN RYN CC-3´. 5`-GAT GCG GCC GCR CTN GAN ACG GTG ACC NGN GAN CC-3´. 5`-GAT GCG GCC GCR CTN GAN ACG GTG ACC NGR CTN CC-3´) introducing SfiI and NotI restriction sites. The $V_HH$ library was subcloned into the SfiI/ NotI sites of the pHEN4 phagemid vector [28]

**$V_HH$ Screening** For the selection of RBD-specific $V_HH$s two consecutive phage enrichment rounds were performed. Therefore, TG1 cells containing the 'immune'-library in pHen4 were infected with the M13K07 helper phage, hence the $V_HH$ domains were presented superficial on phages. For each round 1 x $10^{11}$ phages of the 'immune'-library were applied on RBD either directly coated on immunotubes (10 µg/ml) or biotinylated RBD (5 µg/ml) immobilized on 96-well plates pre-coated with Streptavidin. In each selection round extensive blocking of antigen and phages was performed by using 5% milk or BSA in PBS-T and with increasing panning round PBS-T washing stringency was intensified. Bound phages were eluted in 100 mM tri-ethylamind, TEA (pH 10.0), followed by immediate neutralization with 1 M Tris/HCl (pH 7.4). For phage preparation for following rounds, exponentially growing TG1 cells were infected and spread on selection plates. Antigen-specific enrichment for each round was monitored by comparing colony number of antigen vs. no antigen selection. Following panning 492 individual clones of the second selection round were screened by standard Phage-ELISA procedures using a horseradish peroxidase-labeled anti-M13 monoclonal antibody (GE-Healthcare).

**Protein expression and purification** RBD-specific Nbs were expressed and purified as previously published [29, 30]. For the expression of SARS-CoV-2 proteins (RBD, stabilized homotrimeric Spike and S1 domain) Expi293 cells were applied in agreement to the protocol of Stadlbauer *et al.* [32]. For quality control all purified proteins were analyzed via SDS-PAGE

bioRxiv preprint doi: https://doi.org/10.1101/2020.09.22.308338; this version posted September 22, 2020. The copyright holder for this preprint (which was not certified by peer review) is the author/funder, who has granted bioRxiv a license to display the preprint in perpetuity. It is made available under aCC-BY-NC-ND 4.0 International license.

according to standard procedures. Therefore, protein samples were denaturized (5 min, 95°C) in 2x SDS-sample buffer containing 60 mM Tris/HCl, pH 6.8; 2% (w/v) SDS; 5% (v/v) 2-mercaptoethanol, 10% (v/v) glycerol, 0.02% bromphenole blue. All proteins were visualized by InstantBlue Coomassie (Expedeon) staining. For immunoblotting proteins were transferred on nitrocellulose membrane (Bio-Rad Laboratories) and detection was performed using anti-His primary antibody (Penta-His Antibody, #34660, Qiagen) followed by donkey-anti-mouse secondary antibody labeled with AlexaFluor647 (Invitrogen) using a Typhoon Trio scanner (GE-Healthcare, Freiburg, Germany; excitation 633 nm, emission filter settings 670 nm BP 30).

**Biophysical biolayer interferometry (BLI)** For analyzing the binding affinity of purified Nbs towards RBD biolayer interferometry (BLItz, ForteBio) was performed. Therefore, biotinylated RBD was immobilized on single-use high-precision streptavidin biosensors (SAX) according to manufacturer's protocols. Depending on the affinity of the RBD-Nb interaction, an appropriate concentration range (15.6 nM-2 µM) of Nbs was used. In total for each run four different Nb concentrations were measured as well as a reference run using PBS instead of Nb in the association step. As negative control the GFP-Nb (500 nM) was applied in the binding studies. By this means, global fits were obtained using the BLItzPro software and the global dissociation constant ($K_D$) was calculated. For the epitope competition analysis biotinylated RBD was immobilized on streptavidin sensor in the same fashion as for the affinity measurements. By two consecutive application steps each with association and short dissociation of two different Nbs (500nM) competition binding was performed.

**Bead-based multiplex binding/ competition assay** Purified RBD, S1 domain and homotrimeric Spike of SARS-CoV-2 were covalently immobilized on spectrally distinct populations of carboxylated paramagnetic beads (MagPlex Microspheres, Luminex Corporation, Austin, TX) using 1-ethyl-3-(3-dimethylaminopropyl)carbodiimide (EDC)/ sulfo-N-hydroxysuccinimide (sNHS) chemistry. For immobilization, a magnetic particle processor (KingFisher 96, Thermo Scientific, Schwerte, Germany) was used. Bead stocks were vortexed

bioRxiv preprint doi: https://doi.org/10.1101/2020.09.22.308338; this version posted September 22, 2020. The copyright holder for this preprint (which was not certified by peer review) is the author/funder, who has granted bioRxiv a license to display the preprint in perpetuity. It is made available under aCC-BY-NC-ND 4.0 International license.

thoroughly and sonicated for 15 seconds. Subsequently, 83 µL of 0.065% (v/v) Triton X-100 and 1 mL of bead stock containing 12.5 x $10^7$ beads of one single bead population were pipetted into each well. The beads were then washed twice with 500 µL of activation buffer (100 mM $Na_2HPO_4$, pH 6.2, 0.005% (v/v) Triton X-100) and activated for 20 min in 300 µL of activation mix containing 5 mg/mL EDC and 5 mg/mL sNHS in activation buffer. Following activation, the beads were washed twice with 500 µL of coupling buffer (500 mM MES, pH 5.0, 0.005% (v/v) Triton X-100) and the proteins were added to the activated beads and incubated for 2 h at 21 °C to immobilize the antigens on the surface. Protein-coupled beads were washed twice with 800 µL of wash buffer (1x PBS, 0.005 % (v/v) Triton X-100) and were finally resuspended in 1,000 µL of storage buffer (1x PBS, 1 % (w/v) BSA, 0.05% (v/v) ProClin). The beads were stored at 4°C until further use. For bead-based multiplex assays, individual bead populations were combined into a bead mix.

For the bead-based ACE2 competition binding assay, Nbs were incubated with the bead-mix containing beads coupled with SARS-CoV-2 homotrimeric Spike, RBD and S1 proteins in the presence of biotinylated ACE2 (Sino Biological) competing for the binding of SARS-CoV-2 spike-derived antigens. Single Nbs or Nb combinations were pre-diluted to a concentration of 6.3 µmol/L per Nb in assay buffer. Afterwards, a 4-fold dilution series was made over eight steps in assay buffer containing 160 ng/mL biotinylated ACE2. Subsequently, 25 µL of every dilution was transferred to 25 µL bead-mix in a 96-well half-area plate. The plate was incubated for 2 h at 21 °C, shaking at 750 rpm. Afterwards, the beads were washed using a microplate washer (Biotek 405TS, Biotek Instruments GmbH) to remove unbound ACE2 or Nbs. The beads were then incubated with R-phycoerythrin-labeled streptavidin to detect biotinylated ACE2 that bound to the immobilized antigen for 45 minutes at 21 °C shaking at 750 rpm. Afterwards, the beads were washed again to remove unbound PE-labeled streptavidin. Measurements were performed with a FLEXMAP 3D instrument using the xPONENT Software version 4.3 (settings: sample size: 80 µL, 50 events, Gate: 7,500 – 15,000, Reporter Gain: Standard PMT).

bioRxiv preprint doi: https://doi.org/10.1101/2020.09.22.308338; this version posted September 22, 2020. The copyright holder for this preprint (which was not certified by peer review) is the author/funder, who has granted bioRxiv a license to display the preprint in perpetuity. It is made available under aCC-BY-NC-ND 4.0 International license.

**NeutrobodyPlex: Bead-based multiplex neutralizing antibody detection assay** Based on the recently described automatable multiplex immunoassay by Becker *et al*. [18], the NeutrobodyPlex was developed and similar assay conditions were applied. For the detection of neutralizing serum antibodies the bead-mix containing beads coupled with purified RBD, S1 domain or homotrimeric Spike of SARS-CoV-2 was incubated with Nb combinations (concentrations ranging from 1.26 µM to 0.08 nM for each Nb) and serum samples of convalescent SARS-CoV-2 patients and healthy donors at a 1:400 dilution. As positive control and maximal signal detection per sample, serum only was included and as negative control for Nb binding a SARS-CoV-2-unspecific GFP nanobody (1.26 µM) was used. For comparison of Nb performance the inhibiting mouse antibody (40591-MM43) was applied in concentrations of 0.17 µM to 0.08 nM. Bound serum IgG were detected via anti-human-IgG-PE as previously described [18].

**Hydrogen-Deuterium Exchange**

*RBD Deuteration Kinetics and Epitope Elucidation*

RBD (5 µL, 73 µM) was either incubated with PBS or RBD-specific Nbs (2.5 µL, 2.5 mg/mL in PBS) at 25 °C for 10 min. Deuterium exchange of the pre-incubated nanobody-antigen complex was initiated by dilution with 67.5 µL PBS (150 mM NaCl, pH 7.4) prepared with $D_2O$ and incubation for 5 and 50 minutes respectively at 25 °C. To ensure a minimum of 90% of complex formation, the molar ratio of antigen to Nbs was calculated according to *Kochert et al.* [33] using the affinity constants of 1.37 nM (NM1228), 3.66 nM (NM1226), 3.82 nM (NM1223), 8.23 nM (NM1230) and 8.34 nM (NM1224) determined by BLI analysis. The final $D_2O$ concentration was 90%. After 5 and 50 min at 25 °C, aliquots of 15 µL were taken and quenched by adding 15 µL ice-cold quenching solution (0.2 M TCEP with 1.5% formic acid and 4 M guanidine HCl in 100 mM ammonium formate solution pH 2.2) resulting in a final pH of 2.5. Quenched samples were immediately snap frozen. The immobilized pepsin was prepared by adding 60 µl of 50% slurry (in ammonium formate solution pH 2.5) to a tube and dried by centrifugation at 1000 x g for 3 min at 0 °C and discarding the supernatant. Before injection,

bioRxiv preprint doi: https://doi.org/10.1101/2020.09.22.308338; this version posted September 22, 2020. The copyright holder for this preprint (which was not certified by peer review) is the author/funder, who has granted bioRxiv a license to display the preprint in perpetuity. It is made available under aCC-BY-NC-ND 4.0 International license.

aliquots were thawed and added to the dried pepsin beads. Proteolysis was performed for 2 min in a water ice bath followed by filtration using a 22 µm filter and centrifugation at 1000 x g for 30 s at 0 °C. Samples were immediately injected to a LC-MS system. Undeuterated control samples were prepared under the same conditions using $H_2O$ instead of $D_2O$. The same protocol was applied for the Nbs without addition of RBD as well to create a list of peptic peptides. The HDX experiments of the RBD-Nb-complex were performed in triplicates. The back-exchange of the method as determined using a standard peptide mixture of 14 synthetic peptides was 24%.

*Chromatography and Mass Spectrometry*

HDX samples were analyzed on a LC-MS system comprised of RSLC pumps (UltiMate 3000 RSLCnano, Thermo Fisher Scientific, Dreieich, Germany), a chilling device for chromatography (MéCour Temperature Control, Groveland, MA, USA) and a mass spectrometer Q Exactive (Thermo Fisher Scientific, Dreieich, Germany). The chilling device contained the LC column (ACQUITY BEH C18, 1.7 µm, 300 Å, 1 mm x 50 mm (Waters GmbH, Eschborn, Germany)), a cooling loop for HPLC solvents, a sample loop, and the injection valve and kept them at 0 °C. Samples were analyzed using a two-step 20 min linear gradient with a flow rate of 50 µl/min. Solvent A was 0.1% (v/v) formic acid and solvent B was 80% acetonitrile (v/v) with 0.1% formic acid (v/v). After 3 min desalting at 10% B, a 9 min linear gradient from 10 to 25% B was applied followed by an 8 min linear gradient from 25 to 68.8%. Experiments were performed using a Q Exactive (Thermo Fisher Scientific, Dreieich, Germany) with 70,000 resolutions instrument configurations as follows: sheath gas flow rate of 25; aux gas flow rate of 5; S-lens RF level of 50, spray voltage of 3.5 kV and a capillary temperature of 300 °C.

*HDX Data Analysis*

A peptic peptide list containing peptide sequence, retention time and charge state was generated in a preliminary LC-MS/MS experiment. The peptides were identified by exact mass and their fragment ion spectrum using protein database searches by Proteome Discoverer

bioRxiv preprint doi: https://doi.org/10.1101/2020.09.22.308338; this version posted September 22, 2020. The copyright holder for this preprint (which was not certified by peer review) is the author/funder, who has granted bioRxiv a license to display the preprint in perpetuity. It is made available under aCC-BY-NC-ND 4.0 International license.

v2.1.0.81 (Thermo Fisher Scientific, Dreieich, Germany) and implemented SEQUEST HT search engine. The protein database contained the RBD and the pepsin sequences. Precursor and fragments mass tolerance were set to 6 ppm and 0.05 Da, respectively. No enzyme selectivity was applied, however identified peptides were manually evaluated to exclude peptides originated through cleavage after arginine, histidine, lysine, proline and the residue after proline [34]. FDR was estimated using q-values calculated by Perculator and only peptides with high-confidence identification (q-value ≤ 0.01) were included to the list. Peptides with overlapping mass, retention time and charge in Nb and antigen digest, were manually removed. The deuterated samples were recorded in MS mode only and the generated peptide list was imported into HDExaminer v2.5.0 (Sierra Analytics, Modesto, CA, USA). Deuterium uptake was calculated using the increase of the centroid mass of the deuterated peptides. HDX could be followed for 79% of the RBD amino acid sequence. The calculated percentage deuterium uptake of each peptide between RBD-Nb and RBD-only were compared. Any peptide with uptake reduction of 5% or greater upon Nb binding was considered as protected.

**Cell culture** Caco-2 (Human Colorectal adenocarcinoma) cells were cultured at 37°C with 5% $CO_2$ in DMEM containing 10% FCS, with 2 mM l-glutamine, 100 µg/ml penicillin-streptomycin and 1% NEAA.

**Viruses** All experiments associated with the authentic virus were conducted in Biosafety Level 3 laboratory. The recombinant SARS-CoV-2 expressing mNeonGreen (icSARS-CoV-2-mNG) (PMID: 32289263) was obtained from the World Reference Center for Emerging Viruses and Arboviruses (WRCEVA) at the UTMB (University of Texas Medical Branch). To generate icSARS-CoV-2-mNG stocks, 200.000 Caco-2 cells were infected with 50 µl of virus in a 6-well plate, the supernatant was harvested 48 hpi, centrifuged, and stored at -80°C. For MOI determination, a titration using serial dilutions of the mNeonGreen (icSARS-CoV-2-mNG) was conducted. The number of infectious virus particles per ml was calculated as the (MOI × cell number)/ (infection volume), where MOI = −ln(1 − infection rate).

bioRxiv preprint doi: https://doi.org/10.1101/2020.09.22.308338; this version posted September 22, 2020. The copyright holder for this preprint (which was not certified by peer review) is the author/funder, who has granted bioRxiv a license to display the preprint in perpetuity. It is made available under aCC-BY-NC-ND 4.0 International license.

**Neutralization assay** For neutralization experiments, 1 ×$10^4$ Caco-2 cells/well were seeded in 96-well plates the day before infection in media containing 5% FCS. Caco-2 cells were co-incubated with the SARS-CoV-2 strain icSARS-CoV-2-mNG at a MOI=1.1 and Nbs or serum samples in serial dilutions in the indicated concentrations. 48 hpi cells were fixed with 2% PFA and stained with Hoechst33342 (1 µg/mL final concentration) for 10 minutes at 37°C. The staining solution was removed and exchanged for PBS. For quantification of infection rates, images were taken with the Cytation3 (Biotek) and Hoechst+ and mNG+ cells were automatically counted by the Gen5 Software (Biotek). Data were normalized to respective virus-only infection control. Inhibitory concentration 50 ($IC_{50}$) was calculated as the half-maximal inhibitory dose using 4-parameter nonlinear regression (GraphPad Prism).

**Patient samples** A total of 23 serum samples from SARS-CoV-2 convalescent donors and 4 healthy donors were analyzed in the course of this study. All samples used were de-identified and pre-existing. Ethical consent was granted from the Ethics commission of the University of Tuebingen under the votum 179/2020/BO2. Samples were classified as SARS-CoV-2 infected, due to a self-reported positive SARS-CoV-2 RT-PCR.

**Analyses and Statistics** Graph preparation and statistical analysis was performed using the GraphPad Prism Software (Version 8.3.0).

bioRxiv preprint doi: https://doi.org/10.1101/2020.09.22.308338; this version posted September 22, 2020. The copyright holder for this preprint (which was not certified by peer review) is the author/funder, who has granted bioRxiv a license to display the preprint in perpetuity. It is made available under aCC-BY-NC-ND 4.0 International license.

## Data availability

The data that support the findings of this study are available from the corresponding authors upon reasonable request.

## Authorship Contributions

N.S.M., T.W., M.B. and U.R. designed the study; P.D.K., B.T. T.W. performed Nb selection and biochemical characterization; S.N., A.S. immunized the animals; J.H., D.J., M.B., performed the multiplex binding assay; M.G., A.Z. performed HDX-MS experiments; Mo.S., G.K. A.N., J.S.W. and K.S.L. organize and provide patient samples; N.R.B., M.S. performed viral neutralization assays; T.W., M.B., J.H., M.G., A.Z., N.R.B., M.S. and U.R. analyzed data and performed statistical analysis. T.W. and U.R. drafted the manuscript; N.S.M., U.R. supervised the study. All authors critically read the manuscript.

bioRxiv preprint doi: https://doi.org/10.1101/2020.09.22.308338; this version posted September 22, 2020. The copyright holder for this preprint (which was not certified by peer review) is the author/funder, who has granted bioRxiv a license to display the preprint in perpetuity. It is made available under aCC-BY-NC-ND 4.0 International license.

**Figures:**

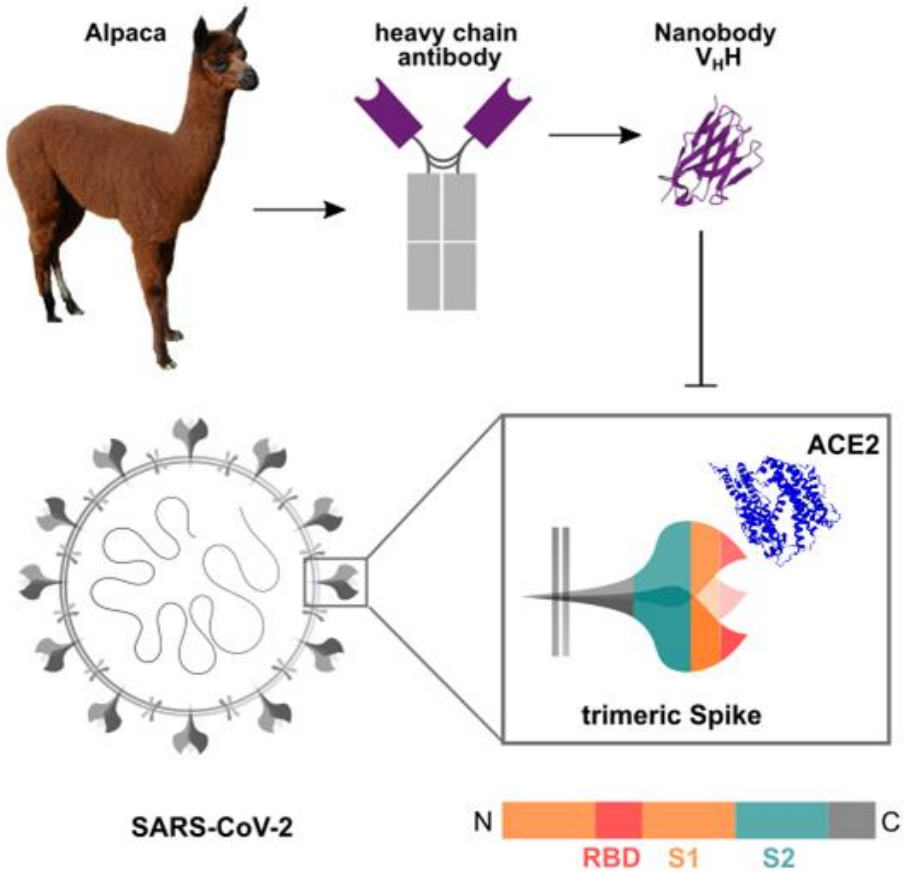


**Figure 1 Schematic depiction of the generation of Nbs blocking the SARS-CoV-2 RBD:ACE2 interaction site**

Nanobodies (Nbs) are genetically engineered from heavy chain only antibodies of alpacas. The interaction between the SARS-CoV-2 homotrimeric Spike protein and ACE2 can be blocked by RBD-specific Nbs. Protein structures adapted from PDB 3OGO (Nb) and 6CS2 (ACE2).

bioRxiv preprint doi: https://doi.org/10.1101/2020.09.22.308338; this version posted September 22, 2020. The copyright holder for this preprint (which was not certified by peer review) is the author/funder, who has granted bioRxiv a license to display the preprint in perpetuity. It is made available under aCC-BY-NC-ND 4.0 International license.

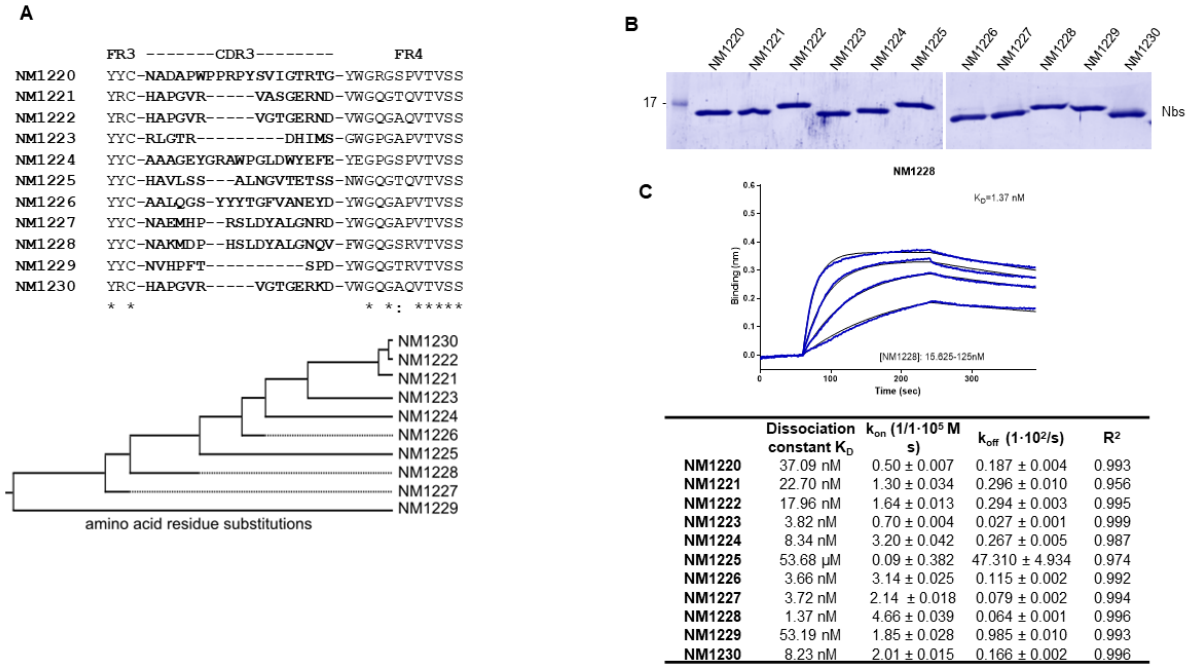


| | Dissociation constant $K_D$ | $k_{on}$ ($1/1 \cdot 10^5$ M s) | $k_{off}$ ($1 \cdot 10^2$/s) | $R^2$ |
|---|---|---|---|---|
| **NM1220** | 37.09 nM | 0.50 ± 0.007 | 0.187 ± 0.004 | 0.993 |
| **NM1221** | 22.70 nM | 1.30 ± 0.034 | 0.296 ± 0.010 | 0.956 |
| **NM1222** | 17.96 nM | 1.64 ± 0.013 | 0.294 ± 0.003 | 0.995 |
| **NM1223** | 3.82 nM | 0.70 ± 0.004 | 0.027 ± 0.001 | 0.999 |
| **NM1224** | 8.34 nM | 3.20 ± 0.042 | 0.267 ± 0.005 | 0.987 |
| **NM1225** | 53.68 µM | 0.09 ± 0.382 | 47.310 ± 4.934 | 0.974 |
| **NM1226** | 3.66 nM | 3.14 ± 0.025 | 0.115 ± 0.002 | 0.992 |
| **NM1227** | 3.72 nM | 2.14 ± 0.018 | 0.079 ± 0.002 | 0.994 |
| **NM1228** | 1.37 nM | 4.66 ± 0.039 | 0.064 ± 0.001 | 0.996 |
| **NM1229** | 53.19 nM | 1.85 ± 0.028 | 0.985 ± 0.010 | 0.993 |
| **NM1230** | 8.23 nM | 2.01 ± 0.015 | 0.166 ± 0.002 | 0.996 |

**Figure 2: Selection of nanobodies (Nbs) against RBD**

**(A)** Amino acid sequences of the complementarity determining region (CDR) 3 from unique Nbs selected after two rounds of biopanning are listed (upper panel). Phylogenetic tree based on a ClustalW alignment of the CDR3 sequences is shown (lower panel). (**B**) Recombinant expression and purification of Nbs using immobilized metal affinity chromatography (IMAC) and size exclusion chromatography (SEC). Coomassie staining of 2 µg of purified Nbs is shown (**C**) For biolayer interferometry (BLI)-based affinity measurements, biotinylated RBD was immobilized on streptavidin biosensors. Kinetic measurements were performed by using four concentrations of purified Nbs ranging from 15.6 nM - 2 µM. As an example the sensogram of NM1228 at indicted concentrations is shown (upper panel). The table summarizes affinities ($K_D$), association ($K_{on}$) and dissociation constants ($K_{off}$) determined for individual Nbs (lower panel).

bioRxiv preprint doi: https://doi.org/10.1101/2020.09.22.308338; this version posted September 22, 2020. The copyright holder for this preprint (which was not certified by peer review) is the author/funder, who has granted bioRxiv a license to display the preprint in perpetuity. It is made available under aCC-BY-NC-ND 4.0 International license.

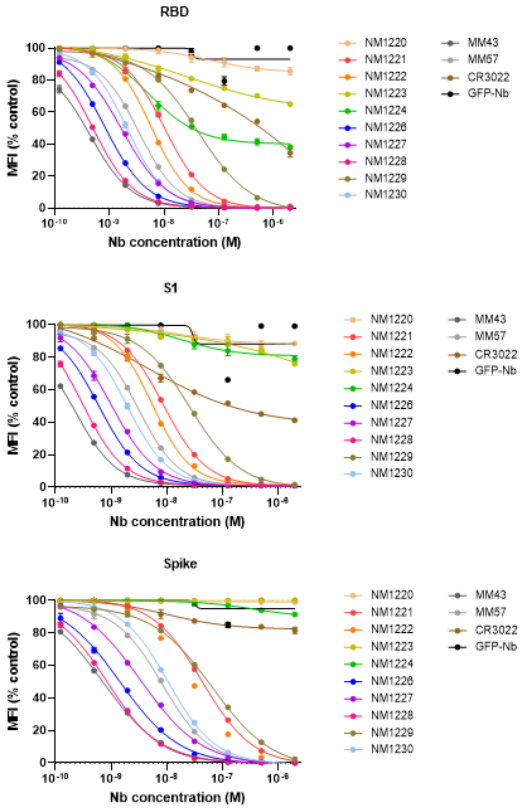


| | $IC_{50}$ (nM) ACE2:RBD Inhibition | $IC_{50}$ (nM) ACE2:S1 Inhibition | $IC_{50}$ (nM) ACE2:Spike Inhibition |
|---|---|---|---|
| **NM1220** | NA | NA | NA |
| **NM1221** | 10.14 | 43.28 | 8.95 |
| **NM1222** | 5.80 | 27.28 | 5.50 |
| **NM1223** | NA | NA | NA |
| **NM1224** | 36.58 | NA | NA |
| **NM1226** | 0.82 | 1.44 | 0.63 |
| **NM1227** | 1.65 | 3.51 | 1.06 |
| **NM1228** | 0.50 | 0.85 | 0.32 |
| **NM1229** | 37.83 | 56.07 | 24.95 |
| **NM1230** | 2.12 | 10.57 | 1.96 |
| **GFP-Nb** | NA | NA | NA |
| **40591-MM43** | 0.38 | 0.71 | 0.20 |
| **40592-MM57** | 3.22 | 7.83 | 2.93 |
| **CR3022** | 585.27 | 2016,00 | 141.26 |

**Figure 3: Multiplex binding assay to identify inhibitory Nbs**

Results from bead-based multiplex ACE2 competition assay are shown for the three SARS-CoV-2 Spike-derived antigens, RBD, S1 and homotrimeric Spike. ACE2 bound to the respective antigen was detected. For each Nb, a dilution series over eight steps (2.106 µM to 0.123 nM) is shown in the presence of 80 ng/mL ACE2. MFI signals were normalized to the maximal signal per antigen as given by the ACE2-only control. $IC_{50}$ values were calculated from a four-parametric sigmoidal model and are displayed for each Nb and antigen. Data are presented as mean +/- stds of three technical replicates (n =3).

bioRxiv preprint doi: https://doi.org/10.1101/2020.09.22.308338; this version posted September 22, 2020. The copyright holder for this preprint (which was not certified by peer review) is the author/funder, who has granted bioRxiv a license to display the preprint in perpetuity. It is made available under aCC-BY-NC-ND 4.0 International license.

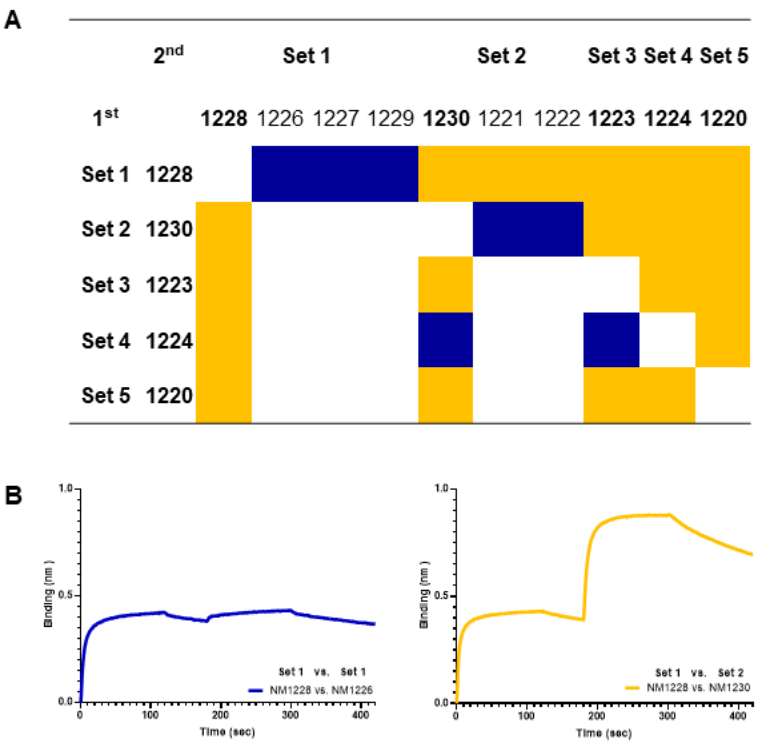


**Figure 4 Epitope binning of Nbs**

(**A**) Heat map illustration of competitive Nb epitope binning on RBD using biolayer interferometry (BLI). Rows and columns represent the loading of the first and second Nb, respectively. Blue colored squares illustrate no additional binding of the second Nb meaning both Nbs belong to the same Nb-Set. Orange colored squares represent additional binding of the second Nb, hence these Nbs belong to different Nb-Sets. (**B**) Representative sensograms of single BLI measurements of Nbs affiliated to the same Nb-Set (NM1228/ NM1226, blue) and to different Nb-Sets (NM1228/ NM1230, orange) are shown.

bioRxiv preprint doi: https://doi.org/10.1101/2020.09.22.308338; this version posted September 22, 2020. The copyright holder for this preprint (which was not certified by peer review) is the author/funder, who has granted bioRxiv a license to display the preprint in perpetuity. It is made available under aCC-BY-NC-ND 4.0 International license.

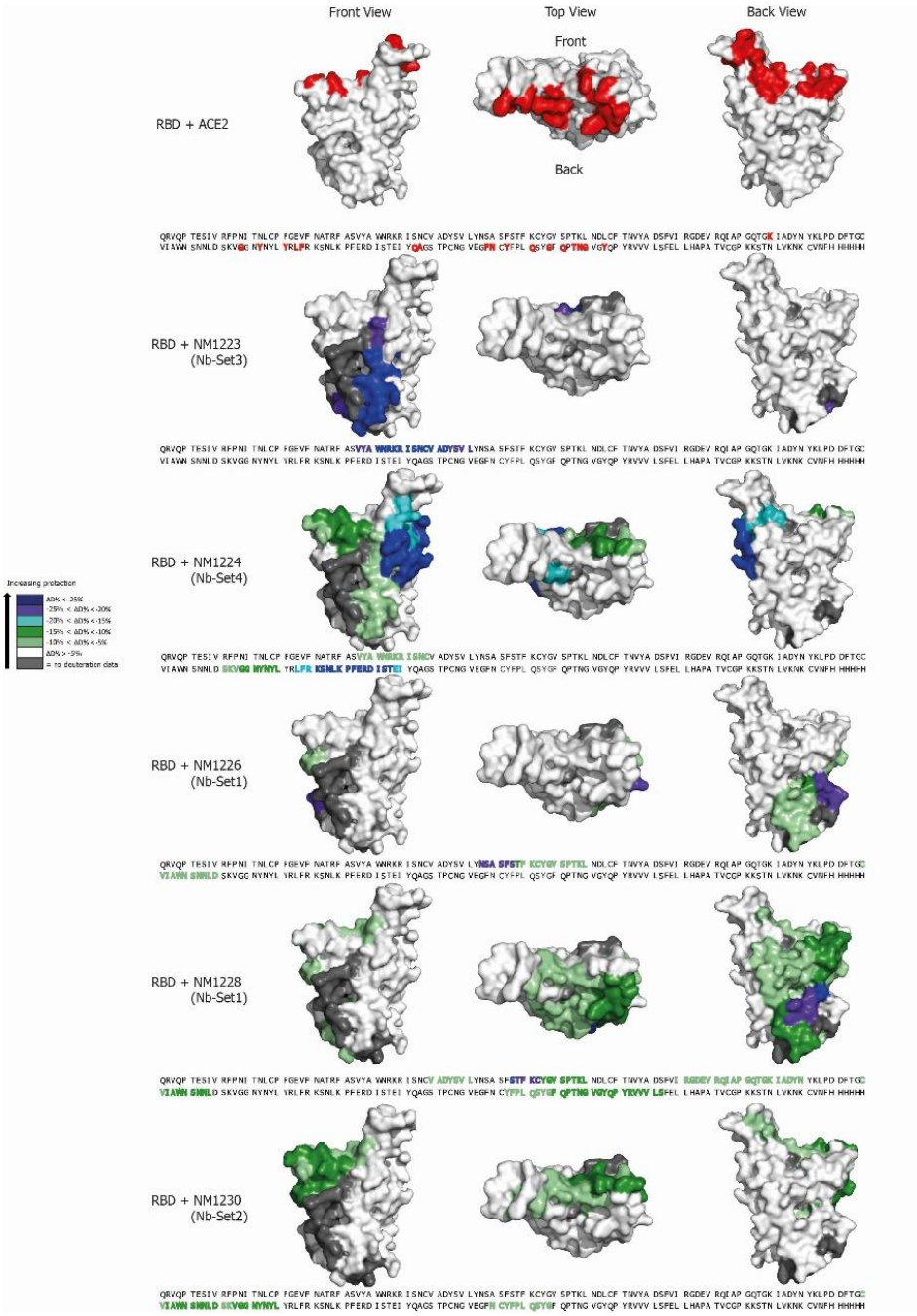


**Figure 5: Epitope mapping of Nbs by HDX mass spectrometry**

Surface structure model of the RBD showing the ACE2 interface and the HDX-MS epitope mapping results of NM1223, NM1224, NM1226, NM1228, NM1230. Amino acid residues of RBD (PDB 6M17 [2]) involved in the RBD:ACE2 interaction site [2, 35] are shown in red (top panel). RBD epitopes protected upon Nb binding are highlighted in different colors indicating the strength of protection. Amino acid residues which are part of the Nb epitopes are highlighted in the RBD sequence.

bioRxiv preprint doi: https://doi.org/10.1101/2020.09.22.308338; this version posted September 22, 2020. The copyright holder for this preprint (which was not certified by peer review) is the author/funder, who has granted bioRxiv a license to display the preprint in perpetuity. It is made available under aCC-BY-NC-ND 4.0 International license.

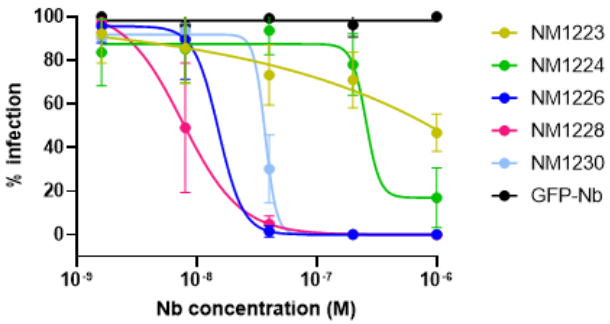


| | $IC_{50}$ (nM) viral neutralization potency |
|---|---|
| **NM1223** | N/A |
| **NM1224** | 256.03 |
| **NM1226** | 15.11 |
| **NM1228** | 7.56 |
| **NM1230** | 37.01 |
| **GFP-Nb** | N/A |

**Figure 6: Viral neutralization potency of selected Nbs**

(**A**) Inhibition of viral infectivity of the SARS-CoV-2 strain icSARS-CoV-2-mNG was analyzed in Caco-2 cells using serial dilutions of NM1223, NM1224, NM1226, NM1228 and NM1230. As negative control GFP-Nb was used. 48 h post-infection neutralization potency was visualized via Hoechst staining and mNeonGreen expression. Intensities of mNeonGreen signal normalized to virus-only infection control are illustrated as percent of infection. $IC_{50}$ values were calculated from a four-parametric sigmoidal model and are displayed for each Nb. Data are presented as mean +/- stds of three technical replicates (n =3).

bioRxiv preprint doi: https://doi.org/10.1101/2020.09.22.308338; this version posted September 22, 2020. The copyright holder for this preprint (which was not certified by peer review) is the author/funder, who has granted bioRxiv a license to display the preprint in perpetuity. It is made available under aCC-BY-NC-ND 4.0 International license.

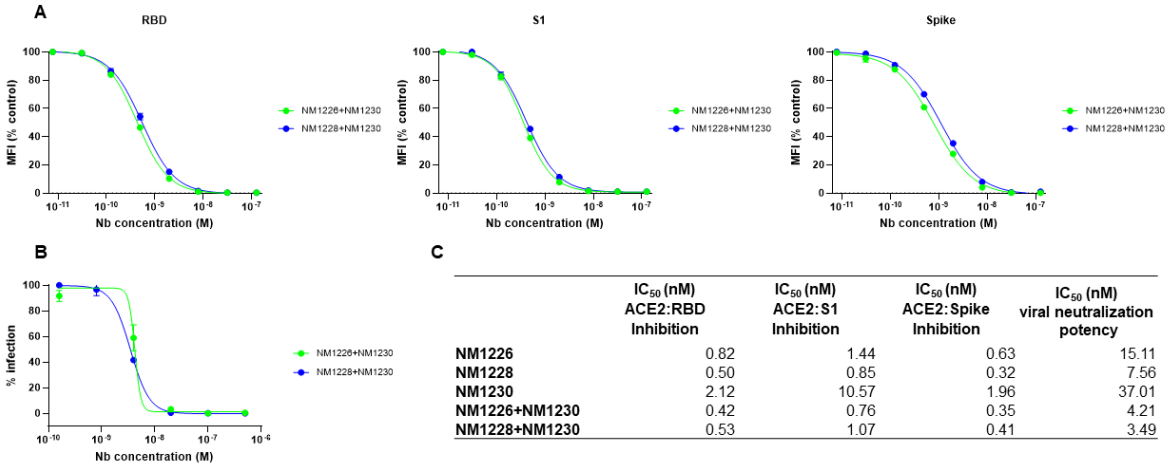


C

| | $IC_{50}$ (nM) ACE2:RBD Inhibition | $IC_{50}$ (nM) ACE2:S1 Inhibition | $IC_{50}$ (nM) ACE2:Spike Inhibition | $IC_{50}$ (nM) viral neutralization potency |
|---|---|---|---|---|
| **NM1226** | 0.82 | 1.44 | 0.63 | 15.11 |
| **NM1228** | 0.50 | 0.85 | 0.32 | 7.56 |
| **NM1230** | 2.12 | 10.57 | 1.96 | 37.01 |
| **NM1226+NM1230** | 0.42 | 0.76 | 0.35 | 4.21 |
| **NM1228+NM1230** | 0.53 | 1.07 | 0.41 | 3.49 |

**Figure 7: Combinatorial application of RBD Nbs for inhibition of ACE2 binding and viral neutralization**

(**A**) Results from multiplex ACE2 competition assay are shown for the three Spike-derived antigens: RBD, S1 and homotrimeric Spike. Nb combinations were diluted from 126 nM to 7.69 pM per Nb in the presence of 80 ng/mL ACE2 and antigen-bound ACE2 was measured. MFI signals were normalized to the maximum detectable signal per antigen given by the ACE2-only control. $IC_{50}$ values were calculated from a four-parametric sigmoidal model. Data are presented as mean +/- stds of three technical replicates (n =3). (**B**) Neutralization potency of Nb-Set1 (NM1226, NM1228) in combination with Nb-Set2 (NM1230) was analyzed in Caco-2 cells using the SARS-CoV-2 strain icSARS-CoV-2-mNG. 48 h post-infection neutralization potency was visualized via Hoechst staining and mNeonGreen expression. Intensities of mNeonGreen signal normalized to virus-only infection control are illustrated as percent of infection. $IC_{50}$ values were calculated from a four-parametric sigmoidal model and are displayed for each Nb. Data are presented as mean +/- stds of two technical replicates (n = 2). (**C**) Table summarizing the $IC_{50}$ values obtained for the individual Nbs (as shown in **Figure 3** and **Figure 6**) and the Nb combinations.

bioRxiv preprint doi: https://doi.org/10.1101/2020.09.22.308338; this version posted September 22, 2020. The copyright holder for this preprint (which was not certified by peer review) is the author/funder, who has granted bioRxiv a license to display the preprint in perpetuity. It is made available under aCC-BY-NC-ND 4.0 International license.

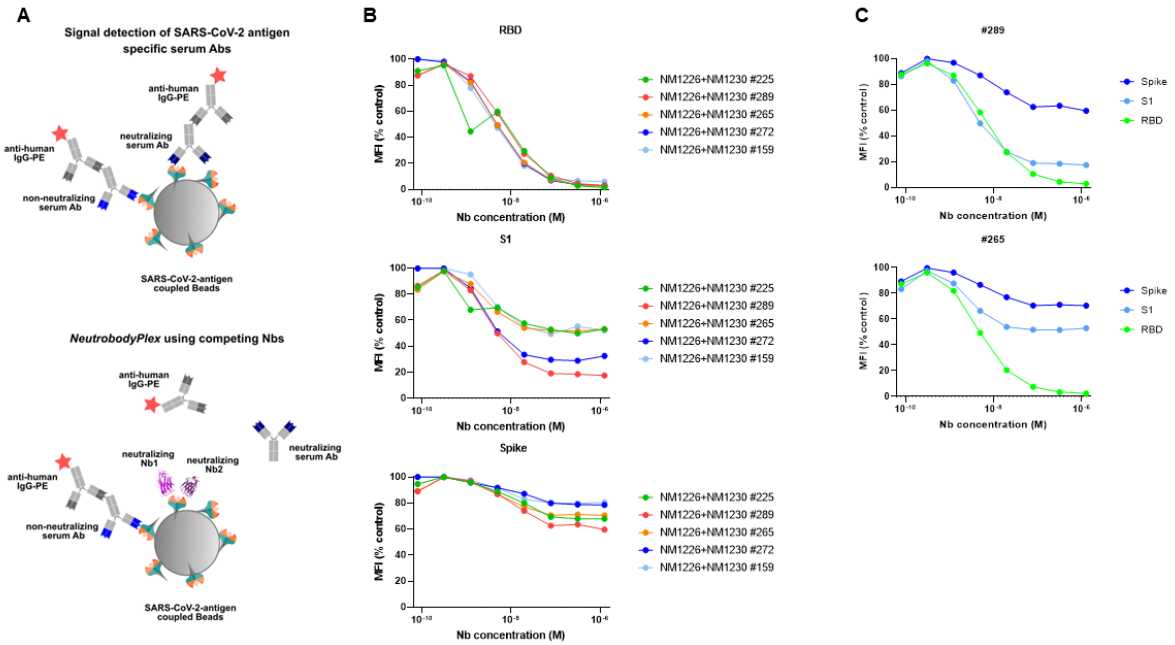


**Figure 8: The NeutrobodyPlex - multiplex competitive binding assay to monitor a neutralizing immune response in patients**

(**A**) Schematic illustration of the NeutrobodyPlex. The replacement of neutralizing IgGs from patient serum from binding to SARS-CoV-2 derived antigens upon addition of RBD Nbs is measured. In presence of neutralizing IgGs, the fluorescent signal from anti-human-IgG-PE, is inversely proportional to the applied Nb concentration. (**B**) For the NeutrobodyPlex assay serial dilutions (1.26 µM to 7.69 pM per Nb) of the combination NM1226/ NM1230 were incubated with five serum samples followed by detection of bound human IgGs. Shown are MFI signals obtained for all three Spike-derived antigens (RBD, S1 domain, homotrimeric Spike) normalized to serum-only control. (**C**) For two serum samples (#289, #265) differences in competition efficiency between the three Spike-derived antigens are shown.

bioRxiv preprint doi: https://doi.org/10.1101/2020.09.22.308338; this version posted September 22, 2020. The copyright holder for this preprint (which was not certified by peer review) is the author/funder, who has granted bioRxiv a license to display the preprint in perpetuity. It is made available under aCC-BY-NC-ND 4.0 International license.

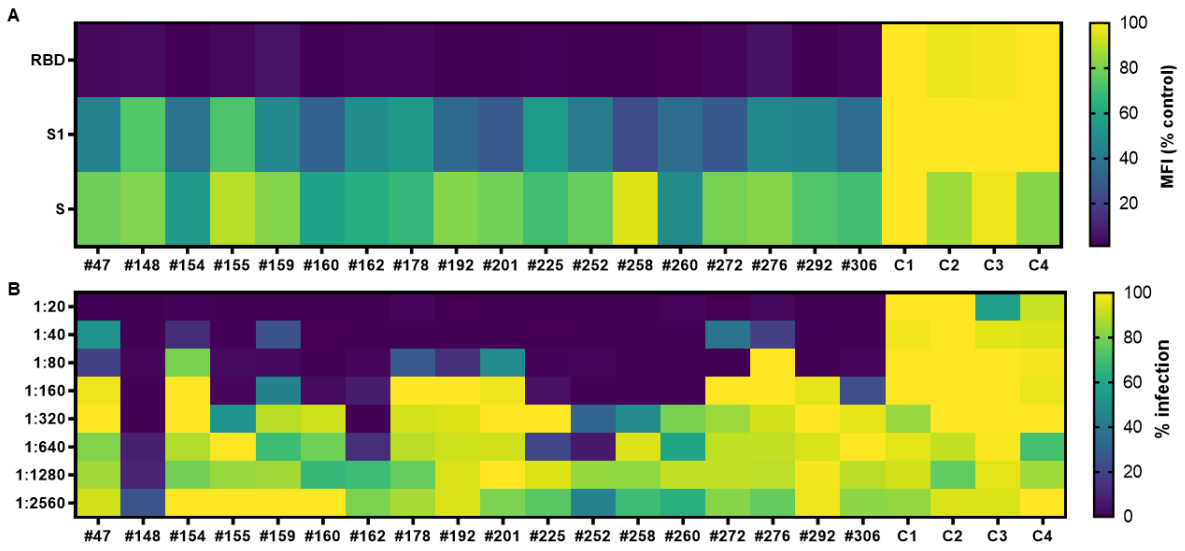


**Figure 9: NeutrobodyPlex validation by testing patient samples in comparison to viral neutralization assay**

(**A**) 18 serum samples from SARS-CoV-2 convalescent patients and four from healthy donors were analyzed using the NeutrobodyPlex with fixed concentration of the Nb combination NM1226/ NM1230 (1.26 µM per Nb). MFI values normalized to serum only control are illustrated as heat map graphic. Dark blue color coding represents loss of the detectable signal, meaning a strong shift of serum antibodies into the unbound state by off-competition of Nbs. Yellow color coding represents no signal differences in presence or absence of Nbs.

(**B**) The same serum samples were analyzed using the viral neutralization assay. By infecting Caco-2 cells with the icSARS-CoV-2-mNG strain in presence of serial dilutions of the serum samples (1:20-1:2560) the neutralization potency was determined via Hoechst staining and mNeonGreen expression 48 h post-infection. Intensities of mNeonGreen signal normalized to virus-only infection control are illustrated as percent of infection in a heat map graphic. Dark blue color represents low mNeonGreen signal, meaning the presence of neutralizing serum antibodies. Yellow color coding represents high mNeonGreen signal, indicating a lower inhibition of viral infection.

bioRxiv preprint doi: https://doi.org/10.1101/2020.09.22.308338; this version posted September 22, 2020. The copyright holder for this preprint (which was not certified by peer review) is the author/funder, who has granted bioRxiv a license to display the preprint in perpetuity. It is made available under aCC-BY-NC-ND 4.0 International license.

## Supplementary Figures

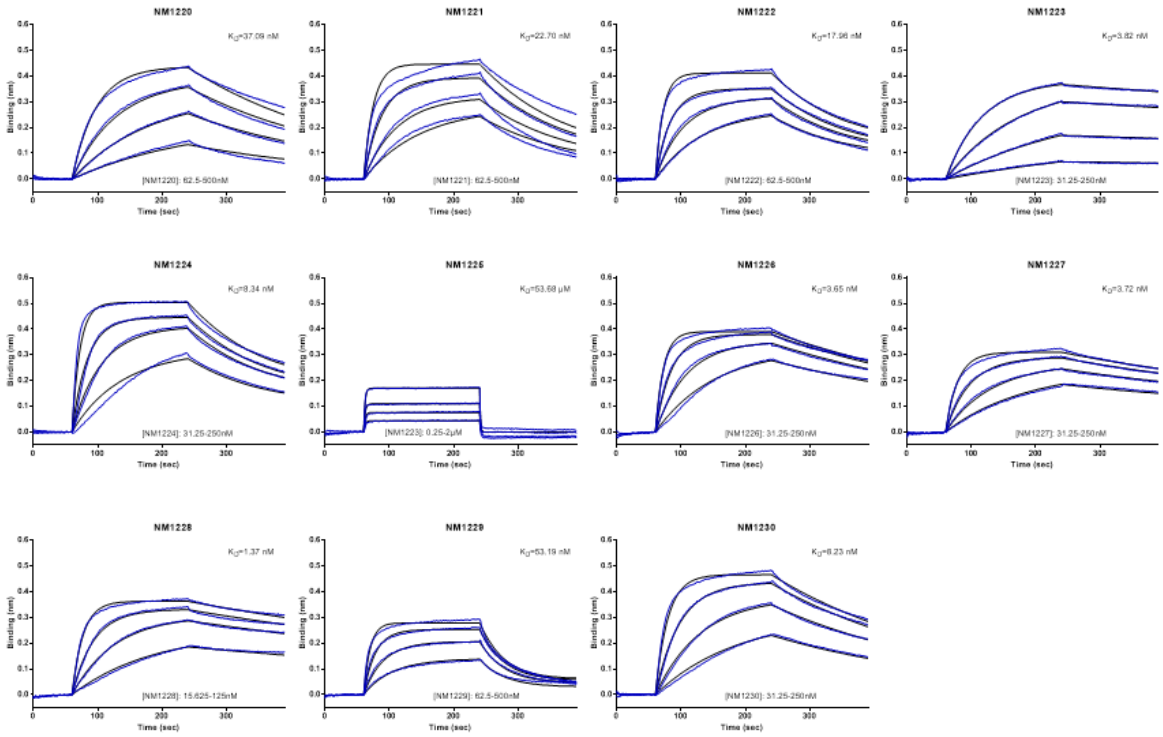


**Supplementary Figure 1: Affinities of RBD binding Nbs determined by biolayer interferometry**

Sensograms of biolayer interferometry-based affinity measurements of 11 identified SARS-CoV-2 RBD Nbs are shown. For analysis biotinylated RBD was immobilized on streptavidin biosensors and kinetic measurements were performed by using four concentrations of purified Nbs ranging from 15.6 nM - 2 µM.

bioRxiv preprint doi: https://doi.org/10.1101/2020.09.22.308338; this version posted September 22, 2020. The copyright holder for this preprint (which was not certified by peer review) is the author/funder, who has granted bioRxiv a license to display the preprint in perpetuity. It is made available under aCC-BY-NC-ND 4.0 International license.

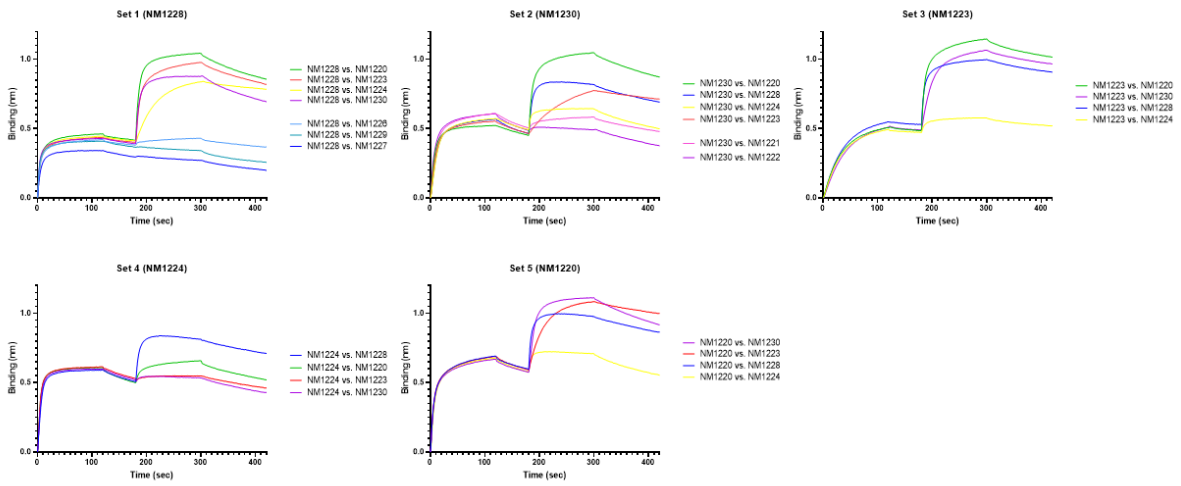


**Supplementary Figure 2: Epitope binning of SARS-CoV-2 RBD Nbs**

Sensograms of biolayer interferometry-based epitope binning of dual Nb binding are shown. Biotinylated RBD was immobilized on streptavidin biosensors followed by two consecutive loading steps of different RBD Nbs. Depending on additional loading (different epitope) or non-loading (similar/ overlapping epitope) of the second Nb, Nbs were clustered into different Nb-Sets. Overall, five Nb-Sets were identified. Set 1: NM1228, NM1226, NM1227, NM1229; Set 2: NM1230, NM1221, NM1222, Set 3: NM1223; Set 4: NM1224; Set 5: NM1220.

bioRxiv preprint doi: https://doi.org/10.1101/2020.09.22.308338; this version posted September 22, 2020. The copyright holder for this preprint (which was not certified by peer review) is the author/funder, who has granted bioRxiv a license to display the preprint in perpetuity. It is made available under aCC-BY-NC-ND 4.0 International license.

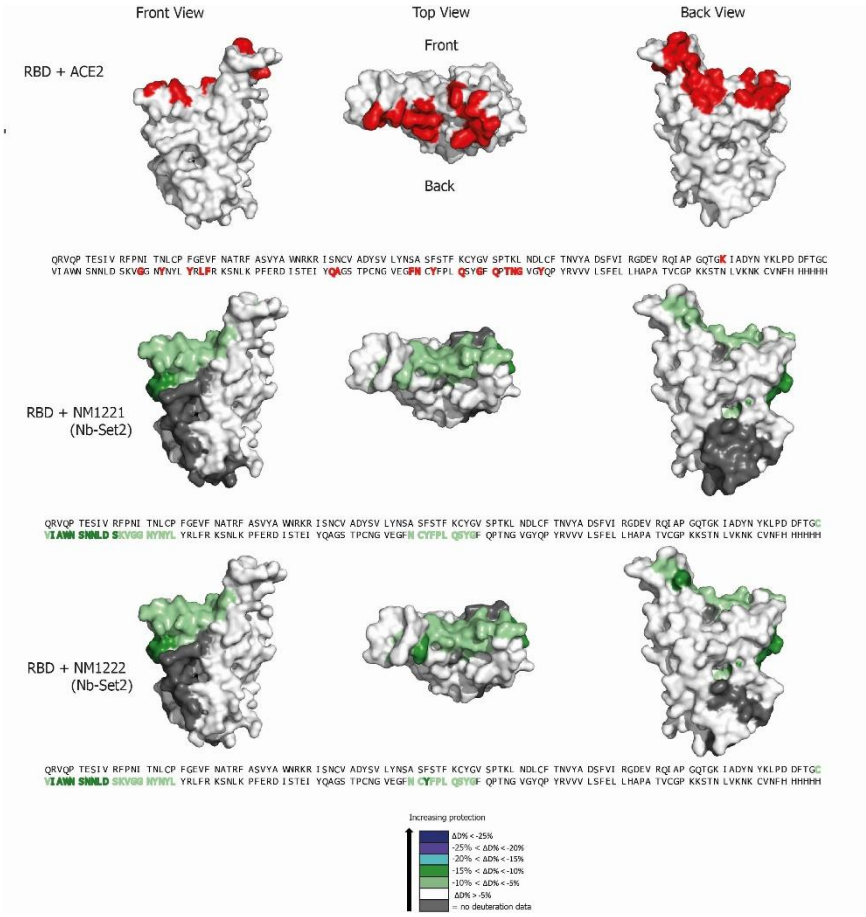


**Supplementary Figure 3 Epitope mapping of Nbs by HDX mass spectrometry**

Surface structure model of the RBD domain showing the ACE2 interface and the HDX-MS epitope mapping results of Nb-Set2. Residues of the RBD (PDB 6M17 [2]) responsible for contact of the ACE2 [2, 35] are shown in red (top panel). RBD epitopes protected upon binding of NM1221, NM1222 and NM1230 are highlighted.

bioRxiv preprint doi: https://doi.org/10.1101/2020.09.22.308338; this version posted September 22, 2020. The copyright holder for this preprint (which was not certified by peer review) is the author/funder, who has granted bioRxiv a license to display the preprint in perpetuity. It is made available under aCC-BY-NC-ND 4.0 International license.

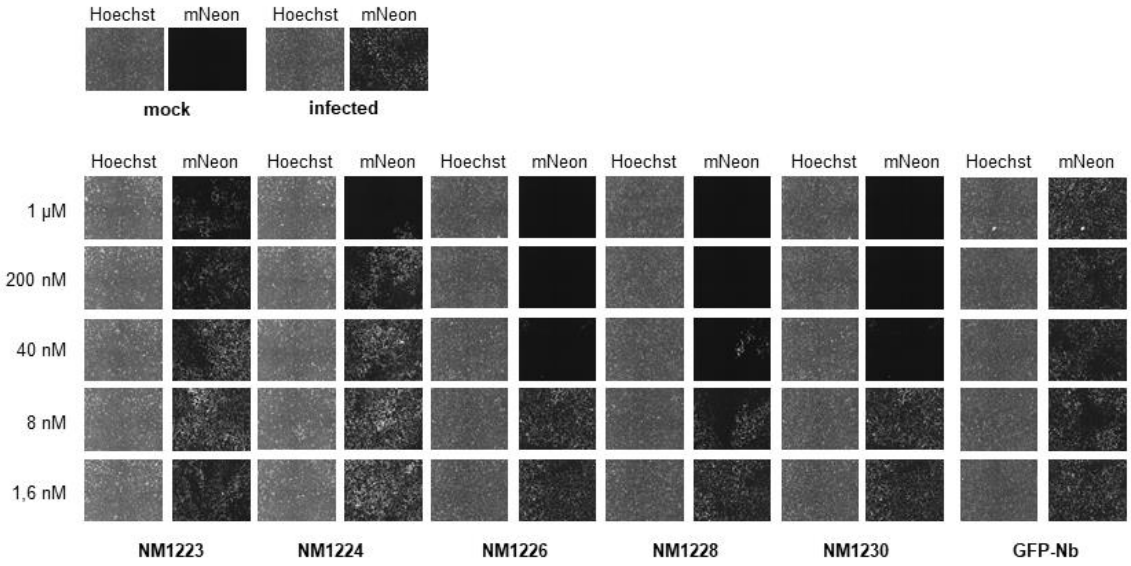


**Supplementary Figure 4: Viral neutralization potency of selected Nbs**

Inhibition of viral infectivity of the SARS-CoV-2 strain icSARS-CoV-2-mNG was analyzed in Caco-2 cells using serial dilutions of NM1223, NM1224, NM1226, NM1228 and NM1230. As negative control the GFP-Nb was used. 48 h post-infection neutralization potency was visualized via Hoechst staining and mNeonGreen expression. Representative images of human Caco-cells upon infection with SARS-CoV-2 expressing mNeonGreen (icSARS-CoV-2-mNG) either in presence or absence of serial dilutions of RBD Nbs are shown.

bioRxiv preprint doi: https://doi.org/10.1101/2020.09.22.308338; this version posted September 22, 2020. The copyright holder for this preprint (which was not certified by peer review) is the author/funder, who has granted bioRxiv a license to display the preprint in perpetuity. It is made available under aCC-BY-NC-ND 4.0 International license.

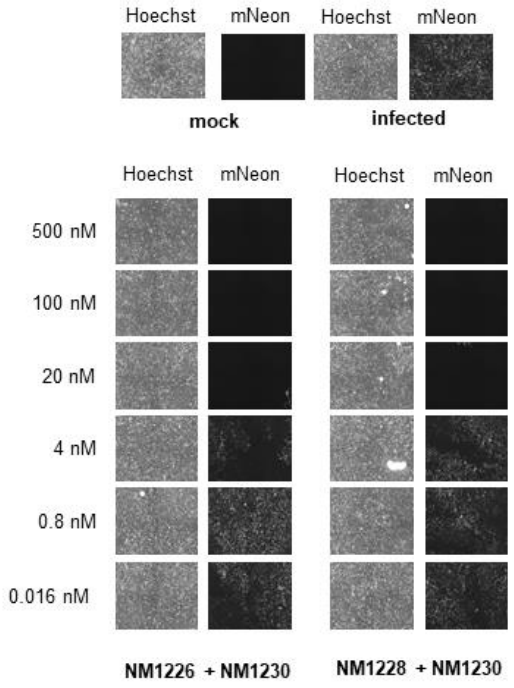


**Supplementary Figure 5: Viral neutralization with Nb combinations**

Inhibition of viral infectivity of the SARS-CoV-2 strain icSARS-CoV-2-mNG was analyzed in Caco-2 cells using serial dilutions of Nb combinations NM1226/ NM1230 and NM1228/ NM1230. 48 h post-infection neutralization potency was visualized via Hoechst staining and mNeonGreen expression. Representative images of human Caco-cells upon infection with SARS-CoV-2 expressing mNeonGreen (icSARS-CoV-2-mNG) either in presence or absence of serial dilutions of combinations of RBD Nbs are shown.

bioRxiv preprint doi: https://doi.org/10.1101/2020.09.22.308338; this version posted September 22, 2020. The copyright holder for this preprint (which was not certified by peer review) is the author/funder, who has granted bioRxiv a license to display the preprint in perpetuity. It is made available under aCC-BY-NC-ND 4.0 International license.

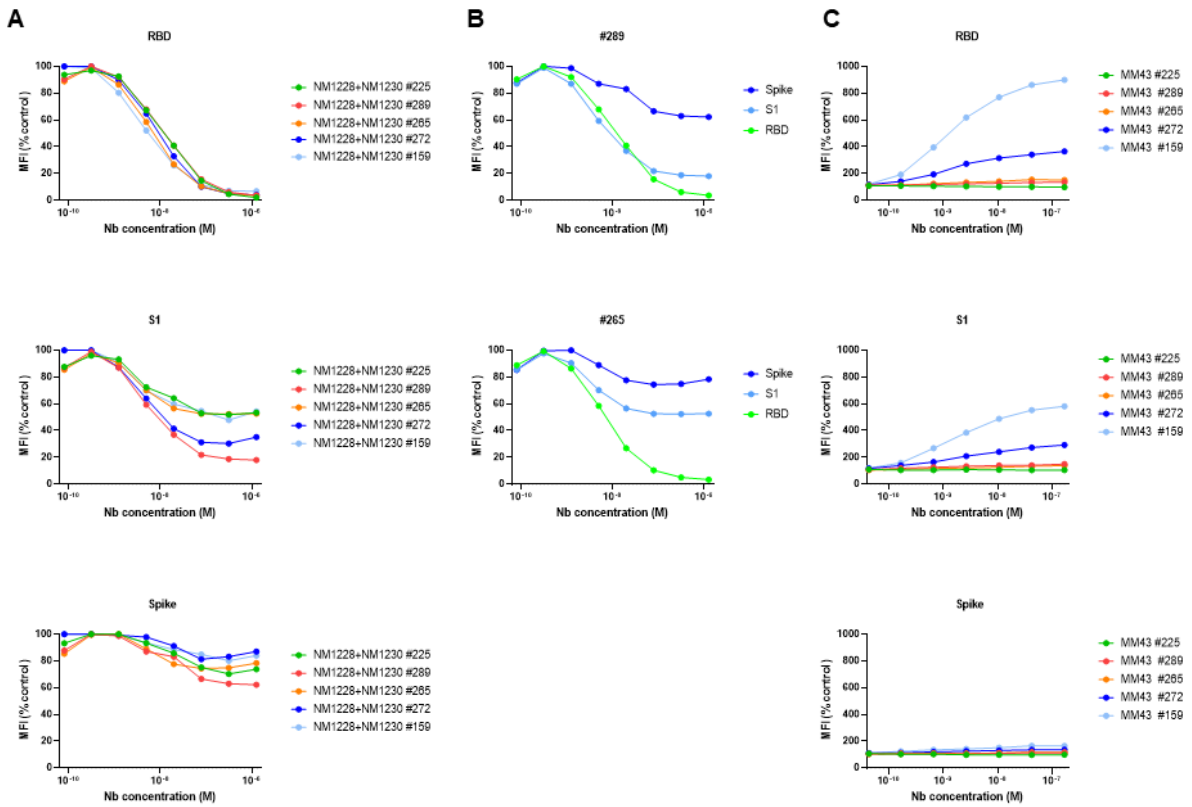


735

736 **Supplementary Figure 6: The NeutrobodyPlex - multiplex competitive binding assay to**

737 **monitor a neutralizing immune response in patients**

738 (**A**) For the NeutrobodyPlex assay serial dilutions (1.26 µM to 7.69 pM per Nb) of the

739 combination NM1228/ NM1230 were incubated with five serum samples followed by detection

740 of bound human IgGs. Shown are MFI signals obtained for all three Spike-derived antigens

741 normalized to serum-only control. (**B**) For two serum samples (#289, #265) differences in Nb

742 competition efficiency between the three Spike based antigens are shown. (**C**) Curves as

743 presented, show normalized MFI signals derived from a similar assay using the neutralizing

744 mouse antibody MM43 in concentrations ranging from of 0.17 µM to 0.08 nM instead of Nb

745 combinations.

746

bioRxiv preprint doi: https://doi.org/10.1101/2020.09.22.308338; this version posted September 22, 2020. The copyright holder for this preprint (which was not certified by peer review) is the author/funder, who has granted bioRxiv a license to display the preprint in perpetuity. It is made available under aCC-BY-NC-ND 4.0 International license.

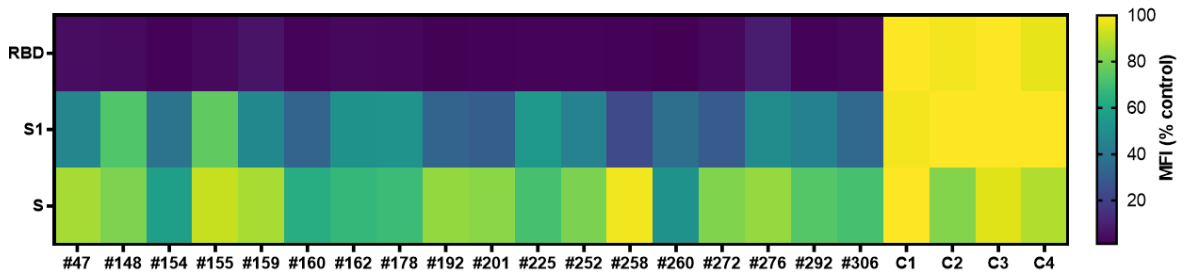


**Supplementary Figure 7: NeutrobodyPlex validation by testing of patient samples**

18 serum samples from SARS-CoV-2 convalescent patients and four from healthy donors were analyzed using the NeutrobodyPlex using a fixed concentration of the Nb combination NM1228/ NM1230 (1.26 µM per Nb). MFI values normalized to serum only control are illustrated as heat map graphic. Dark blue color coding represents loss of the detectable signal, meaning a strong shift of serum antibodies into the unbound state by off-competition of Nbs. Yellow color coding represents no signal differences in presence or absence of Nbs.

bioRxiv preprint doi: https://doi.org/10.1101/2020.09.22.308338; this version posted September 22, 2020. The copyright holder for this preprint (which was not certified by peer review) is the author/funder, who has granted bioRxiv a license to display the preprint in perpetuity. It is made available under aCC-BY-NC-ND 4.0 International license.

## References


1. Rogers, T.F., et al., *Isolation of potent SARS-CoV-2 neutralizing antibodies and protection from disease in a small animal model.* Science, 2020. **369**(6506): p. 956-963.
2. Yan, R., et al., *Structural basis for the recognition of SARS-CoV-2 by full-length human ACE2.* Science, 2020. **367**(6485): p. 1444-1448.
3. Ju, B., et al., *Human neutralizing antibodies elicited by SARS-CoV-2 infection.* Nature, 2020. **584**(7819): p. 115-119.
4. Tai, W., et al., *Characterization of the receptor-binding domain (RBD) of 2019 novel coronavirus: implication for development of RBD protein as a viral attachment inhibitor and vaccine.* Cell Mol Immunol, 2020. **17**(6): p. 613-620.
5. Muyldermans, S., *Nanobodies: natural single-domain antibodies.* Annu Rev Biochem, 2013. **82**: p. 775-97.
6. Wrapp, D., et al., *Structural Basis for Potent Neutralization of Betacoronaviruses by Single-Domain Camelid Antibodies.* Cell, 2020.
7. Huo, J., et al., *Neutralizing nanobodies bind SARS-CoV-2 spike RBD and block interaction with ACE2.* Nat Struct Mol Biol, 2020.
8. Schoof, M., et al., *An ultra-high affinity synthetic nanobody blocks SARS-CoV-2 infection by locking Spike into an inactive conformation.* bioRxiv, 2020.
9. Chi, X., et al., *Humanized Single Domain Antibodies Neutralize SARS-CoV-2 by Targeting Spike Receptor Binding Domain.* bioRxiv, 2020: p. 2020.04.14.042010.
10. Hanke, L., et al., *An alpaca nanobody neutralizes SARS-CoV-2 by blocking receptor interaction.* bioRxiv, 2020: p. 2020.06.02.130161.
11. Esparza, T.J., et al., *High Affinity Nanobodies Block SARS-CoV-2 Spike Receptor Binding Domain Interaction with Human Angiotensin Converting Enzyme.* bioRxiv, 2020: p. 2020.07.24.219857.

bioRxiv preprint doi: https://doi.org/10.1101/2020.09.22.308338; this version posted September 22, 2020. The copyright holder for this preprint (which was not certified by peer review) is the author/funder, who has granted bioRxiv a license to display the preprint in perpetuity. It is made available under aCC-BY-NC-ND 4.0 International license.

12. Nieto, G.V., et al., *Fast isolation of sub-nanomolar affinity alpaca nanobody against the Spike RBD of SARS-CoV-2 by combining bacterial display and a simple single-step density gradient selection.* bioRxiv, 2020: p. 2020.06.09.137935.

13. Xiang, Y., et al., *Versatile, Multivalent Nanobody Cocktails for Highly Efficient SARS-CoV-2 Neutralization.* bioRxiv, 2020: p. 2020.08.24.264333.

14. Gai, J., et al., *A potent neutralizing nanobody against SARS-CoV-2 with inhaled delivery potential.* bioRxiv, 2020: p. 2020.08.09.242867.

15. Korber, B., et al., *Spike mutation pipeline reveals the emergence of a more transmissible form of SARS-CoV-2.* bioRxiv, 2020: p. 2020.04.29.069054.

16. Korber, B., et al., *Tracking Changes in SARS-CoV-2 Spike: Evidence that D614G Increases Infectivity of the COVID-19 Virus.* Cell, 2020. **182**(4): p. 812-827 e19.

17. Amanat, F., et al., *A serological assay to detect SARS-CoV-2 seroconversion in humans.* Nat Med, 2020. **26**(7): p. 1033-1036.

18. Becker, M., et al., *Going beyond clinical routine in SARS-CoV-2 antibody testing - A multiplex corona virus antibody test for the evaluation of cross-reactivity to endemic coronavirus antigens.* medRxiv, 2020: p. 2020.07.17.20156000.

19. Gorshkov, K., et al., *Quantum Dot-Conjugated SARS-CoV-2 Spike Pseudo-Virions Enable Tracking of Angiotensin Converting Enzyme 2 Binding and Endocytosis.* ACS Nano, 2020.

20. Lassaunière, R., et al., *Evaluation of nine commercial SARS-CoV-2 immunoassays.* medRxiv, 2020: p. 2020.04.09.20056325.

21. Robbiani, D.F., et al., *Convergent antibody responses to SARS-CoV-2 in convalescent individuals.* Nature, 2020. **584**(7821): p. 437-442.

22. Roxhed, N., et al., *A translational multiplex serology approach to profile the prevalence of anti-SARS-CoV-2 antibodies in home-sampled blood.* medRxiv, 2020: p. 2020.07.01.20143966.

23. Muruato, A.E., et al., *A high-throughput neutralizing antibody assay for COVID-19 diagnosis and vaccine evaluation.* Nat Commun, 2020. **11**(1): p. 4059.

bioRxiv preprint doi: https://doi.org/10.1101/2020.09.22.308338; this version posted September 22, 2020. The copyright holder for this preprint (which was not certified by peer review) is the author/funder, who has granted bioRxiv a license to display the preprint in perpetuity. It is made available under aCC-BY-NC-ND 4.0 International license.

24. Cao, Y., et al., *Potent Neutralizing Antibodies against SARS-CoV-2 Identified by High-Throughput Single-Cell Sequencing of Convalescent Patients' B Cells.* Cell, 2020. **182**(1): p. 73-84 e16.

25. Chi, X., et al., *A neutralizing human antibody binds to the N-terminal domain of the Spike protein of SARS-CoV-2.* Science, 2020. **369**(6504): p. 650-655.

26. Rothbauer, U., *Speed up to find the right ones: rapid discovery of functional nanobodies.* Nat Struct Mol Biol, 2018. **25**(3): p. 199-201.

27. Tan, C.W., et al., *A SARS-CoV-2 surrogate virus neutralization test based on antibody-mediated blockage of ACE2-spike protein-protein interaction.* Nat Biotechnol, 2020. **38**(9): p. 1073-1078.

28. Arbabi Ghahroudi, M., et al., *Selection and identification of single domain antibody fragments from camel heavy-chain antibodies.* FEBS Lett, 1997. **414**(3): p. 521-6.

29. Kirchhofer, A., et al., *Modulation of protein properties in living cells using nanobodies.* Nat Struct Mol Biol, 2010. **17**(1): p. 133-8.

30. Rothbauer, U., et al., *A versatile nanotrap for biochemical and functional studies with fluorescent fusion proteins.* Mol Cell Proteomics, 2008. **7**(2): p. 282-9.

31. Rothbauer, U., et al., *Targeting and tracing antigens in live cells with fluorescent nanobodies.* Nat Methods, 2006. **3**(11): p. 887-9.

32. Stadlbauer, D., et al., *SARS-CoV-2 Seroconversion in Humans: A Detailed Protocol for a Serological Assay, Antigen Production, and Test Setup.* Curr Protoc Microbiol, 2020. **57**(1): p. e100.

33. Kochert, B.A., et al., *Hydrogen-Deuterium Exchange Mass Spectrometry to Study Protein Complexes.* Methods Mol Biol, 2018. **1764**: p. 153-171.

34. Hamuro, Y. and S.J. Coales, *Optimization of Feasibility Stage for Hydrogen/Deuterium Exchange Mass Spectrometry.* J Am Soc Mass Spectrom, 2018. **29**(3): p. 623-629.

35. Lan, J., et al., *Structure of the SARS-CoV-2 spike receptor-binding domain bound to the ACE2 receptor.* Nature, 2020. **581**(7807): p. 215-220.